ECMWF Workshop on Fine-scale Modelling and the Development of Parametrization Schemes, Reading, 16 to 18 September 1991. (Version of August 20, 1991).

SIMULATIONS AND PARAMETRIZATIONS OF LARGE EDDIES IN CONVECTIVE ATMOSPHERIC BOUNDARY LAYERS

Ulrich Schumann

Deutsche Forschungsanstalt für Luft- und Raumfahrt (DLR)
Institut für Physik der Atmosphäre
Oberpfaffenhofen, Germany

Summary: The paper reviews the method of large-eddy simulation (LES) and its applications to the convective boundary layer (CBL) in the atmosphere at weak mean winds. Simple conceptual models are deduced to explain and parametrize the mean variances and diffusivites over homogeneous and wavy terrain with variable surface heat flux.

1. INTRODUCTION

The purpose of this paper is to review the method of large-eddy simulation (LES), its applications to various dry convective atmospheric boundary layers, and to describe some parametrizations of flow properties which have been deduced from such simulations and related simple models.

As summarized in section 2, a large amount of experiences has been gained in LES. Section 3 reviews applications of LES to CBL, which often prevails over land during day and over relatively warm sea surfaces. Here, we show that very simple models can be derived to explain some of the observations. In section 4 we investigate the effects of wavy terrain and inhomogeneous surface heating. Here the state of knowledge is far less complete than for the homogeneous CBL. Again, simple models may help to determine the impact of surface inhomogeneities, and to derive parametrizations for larger scale models. Many references to related studies are included.

2. THE LES METHOD

2.1 The basic approach

The first successful LES was performed by Deardorff (1970a). The term LES was introduced by Leonard (1974) and Ferziger (1977). Earlier papers referred to the same method as direct numerical simulation (Schumann 1975), but this term is now restricted to solutions of the full Navier Stokes equations that compute the evolution of all significant scales of motion without any turbulence models (Reynolds 1990).

A LES method computes the three-dimensional time-dependent details of the large eddies using a simple subgrid-scale (SGS) model for the effects of the small eddies on the large eddies. Here, the large eddies are those motion elements in a turbulent flow which carry most of the kinetic energy and most of the turbulent fluxes. These motions are simulated using a three-dimensional time-dependent numerical integration scheme which numerically resolves scales in between a lower limit of order h as given by the grid-scale or any equivalent resolution limit of the numerical integration scheme, and an upper limit as given by the size of the computational domain. We require the size of the domain to be large in comparison to the scale of the most energetic motion elements, i.e. the "large

eddies." This is necessary not only to get the correct solutions but also to get sufficient data for reliable statistics (Lenschow and Stankov, 1986). The scale h has to be smaller than the scale of the large eddies. If the grid scale h is close to the scale of the most energetic motions, such a simulation is called a "very large eddy simulation (VLES)" (Reynolds 1990). A VLES demands for more accurate SGS models than a LES in which the SGS fluxes and variances are small. Such a VLES will still be more accurate than a turbulence model which tries to describe all scales of motion together in one model.

The numerical scheme approximates the basic equations which describe the motions in the flow under consideration together with proper boundary and initial conditions. Here we rely on the assumptions that, for flows which approach an asymptotic state, the statistics of the resultant flow are independent of details in the initial conditions. The boundary conditions have to be suitably selected to describe the forcing from larger scales but to let the internal dynamics of turbulent motions unconstrained, which is particularly demanding at inflow and outflow boundaries (Friedrich and Arnal 1990).

The SGS model is necessary because of the nonlinearities of the basic equations. This is formally shown by averaging or filtering the basic equations with respect to motion scales smaller than h. The procedure results into the equations to be solved for the large eddies. Various filter methods have been proposed (Aldama 1990), including volume mean averages (Lilly 1967, Deardorff 1970a), a volume balance method which integrates where possible and identifies SGS contributions as surface mean values (Schumann 1975, Grötzbach 1986, Friedrich and Arnal 1990), and a Gaussian filter within a convolution integral which corresponds to a sharp cut-off in wavenumber space (Leonard 1974). When the filter width is narrow, the effective filter is dictated by the approximation properties of the numerical scheme. Germano (1991) shows that the details of such filters are unimportant. What counts are the scales which are resolved in contrast to the subgrid scales which are to be modelled. On the other hand, Mason and Callen (1986) advocated to use a filter which has a width considerably larger than the grid scale in order to obtain smooth fields which can be numerically approximated without approximation errors.

I believe that this is not necessary. In contrary, one should try to simulate an as large fraction of the turbulent motion energy as possible even if part of the simulations are affected by some second order finite difference error. This is demanding enough as the following estimate shows: If the spectrum of kinetic energy follows the well-known von Karman shape with arbitrary amplitude C, $E(k) = C(k/k_0)^4[1 + (k/k_0)^2]^{-17/6}$ where $k_0 \cong k_{max}/1.6$ is a wavenumber close to that of maximum kinetic energy k_{max}, then one finds by simple integration that all scales up to $k/k_0 \cong 55.4$ (19.5) need to be resolved in order to resolve 90 % (80 %) of all energy. Hence, an order of 50 (20) grid points is the minimum which one should have available to resolve most of the energy. In three dimensions this gives already quite a large number of grid points and, therefore, one cannot afford to provide further grid points (say a factor of 3 more in each dimension) in order to resolve the large scales without any appreciable finite difference errors.

The SGS fluxes have to be modelled. The model must simulate the transfer of kinetic energy and scalar variances from large to small eddies, where the dissipation by molecular diffusion takes place. For high Reynolds numbers (Peclet numbers) and remote from rigid boundaries, these models are usually constructed assuming that the turbulence at

subgrid scales corresponds to Kolmogorov's inertial range of turbulence (Lilly 1967). This requires also that the scale h is small in comparison to the buoyancy scale (Deardorff 1980, Schumann 1991a).

Accurate modelling of the fluxes itself is necessary only where the SGS fluxes get large in comparison to the resolved fluxes. This is typically the case at rigid surfaces where the scales of the most energetic and flux carrying motions tend to zero. At such boundaries a LES actually becomes a VLES. Moreover, for some applications it might be important that the SGS model mimics the stochastic forcing from the small scale motion onto the large eddies (Mason and Thomson 1991). As any turbulence model, the SGS model must satisfy the usual requirements like the correct dimensional and tensorial properties, invariance with respect to Galilean transformations of the coordinate system (Speziale 1985), and realizability (Schumann 1977, 1991a).

Common model variants are the Smagorinsky-Lilly model (Lilly 1967, Deardorff 1970a, 1971), using turbulent diffusivities which depend on the square of the filter scale and the deformation magnitude of the resolved velocity field, the first-order closure model of Prandtl-Kolmogorov type in which the diffusivity is computed as the product of filter scale times square-root of the turbulent kinetic energy of the SGS motions (Schumann 1975, 1991a, Deardorff 1980, Wyngaard and Brost 1984, Moeng 1984, Haren and Nieuwstadt 1989), and second-order closure models which apply the transport equations of the fluxes (Deardorff 1973) or algebraic approximations (Sommeria 1976, Schemm and Lipps 1976, Schmidt and Schumann 1989). Mason (1989) and Mason and Derbyshire (1990) apply the Smagorinsky model with a damping function depending on the local Richardson number, similarly to that proposed by Lilly (1962). I prefer the first-order closure which makes use of an energy transport equation because this equation accounts explicitly for the buoyant forcing and for local deviations from equilibrium, is easy to implement, free of realizability problems, does not require to specify explicitly the critical Richardson number, and apparantly provides as accurate simulations as second-order closures (Schumann 1991a). If the LES is successfully simulating the basic flow, then a factor of two increase in resolution certainly gives better results than any improvement in the SGS model.

Near the surface, the SGS model must be consistent with standard properties of surface layers. E.g. in the Prandtl layer, for high Reynolds number flows, we assume that the shear stress is related to the flow velocity in the first grid point. In neutrally stratified flows, the logarithmic law of the wall describes that relation. By this means also effects of surface roughness get included. For stably or unstably stratified flows, Monin-Obukhov similarity is used as e.g in Schmidt and Schumann (1989). Such rather simple boundary conditions assume that the fluxes at the surface are in phase with the local velocity or other fields in the first grid cell (Schumann 1975). This approach gives results which are very close to various alternative schemes, at least for high Reynolds number flows (Piomelli et al. 1989).

The numerical scheme must simulate correctly the dynamics of the large eddies (Ferziger 1977, 1987). In particular it should be able to account for the tendency to local isotropy (which requires about isotropic resolution) and its approximation errors should be small in comparison to SGS effects (which requires at least second order accuracy because the SGS diffusivities scale with $h^{4/3}$ in the inertial range of turbulence). The numerical scheme

should satisfy integral conservation of mass, momentum and second order moments (kinetic energy and variances) to simulate the dynamics of the large eddies correctly. Such schemes exist for simulations of momentum and scalar fluctuations in incompressible fluids (e.g. Lilly 1965, Piacsek and Williams 1970, Ferziger 1987, Schumann 1975, 1985). The pressure field has to be determined such that the flow satisfies the continuity equation, a task which is easy to accomplish using fast elliptic solvers on regular Cartesian grids (Schumann 1980, Schumann and Sweet 1988) but computationally more demanding in curvilinear coordinates and grids with variable grid spacing in more than just one coordinate (Clark 1977, Schumann and Volkert 1984, Krettenauer 1991). However, for scalar quantities, like water concentrations in cloud models (Deardorff 1980, Moeng 1986), species concentrations in models with chemical reactions (Schumann 1989), or kinetic energy as used for SGS modelling, it is essential that the model guarantees positivity of the scalars. A prominent example of such a scheme is that given by Smolarkiewicz (1984). A refined method is described in Smolarkiewicz and Grabowski (1990) which avoids not only the appearance of negative values but also that of non-physical overshootings. Unfortunately, a scheme which guarantees positivity and, at the same time, conservation of variances is not known so that compromises are unavoidable in this respect. The Smolarkiewicz scheme conserves variances to a higher degree when applied to a scalar with small fluctuations relative to a large mean value (Smolarkiewicz and Clark 1986, Schumann et al. 1987). Hence, one can often optimize the simulations with respect to the conflicting demands of positivity and variance conservation by proper selection of the mean value of the scalar when the mean value itself is irrelevant. This is typically the case for temperature in a Boussinesq fluid and for inert tracers (Ebert et al. 1989). Often, large finite difference errors occur if the flow velocity possesses a large mean value relative to the fluctuating components. For such cases, if ever possible, a Galilean transformation should be used, i.e. a grid which moves with the mean velocity (Deardorff 1970a). Otherwise, the time step has to be taken very small and the discretization errors get large. This may have strong effects on the computed spectrum of turbulence and the energy transfer as measured by velocity derivative skewness (Schumann and Friedrich 1987). Alternatively, the mean advection should be treated by a higher order numerical scheme, e.g. by a pseudospectral method (Rogallo and Moin 1984, Moeng 1984, Gerz et al. 1989).

2.2 Large eddy simulation model equations

For a dry Boussinesq fluid, for small Coriolis forces, at high Reynolds number, the equations to be solved by means of LES are the continuity equation for constant density ρ,

$$\frac{\partial \overline{u}_j}{\partial x_j} = 0 , \tag{1}$$

the equations of motion,

$$\frac{\partial \overline{u}_i}{\partial t} + \frac{\partial (\overline{u}_j \overline{u}_i)}{\partial x_j} = -\frac{1}{\rho} \frac{\partial \overline{p}}{\partial x_i} - \frac{\partial}{\partial x_j} \overline{u''_i u''_j} + \beta g_i \overline{T} , \tag{2}$$

the heat balance (T corresponds to the potential temperature in the Boussinesq approximation), and possibly many budget equations for all scalars ψ involved,

$$\frac{\partial \overline{T}}{\partial t} + \frac{\partial(\overline{u}_j \overline{T})}{\partial x_j} = -\frac{\partial}{\partial x_j}\overline{u''_j T''}, \quad \frac{\partial \overline{\psi}}{\partial t} + \frac{\partial(\overline{u}_j \overline{\psi})}{\partial x_j} = -\frac{\partial}{\partial x_j}\overline{u''_j \psi''}. \tag{3}$$

For flow over smooth orography $h(x, y)$ a transformation is used with z replaced by η, where

$$\eta = H(z - h)/(H - h), \tag{4}$$

and H is the height of the top of the computational domain. This is a standard procedure and described in detail by Clark (1977) and Krettenauer and Schumann (1991).

2.3 Numerical method

The equations are solved numerically using a finite difference scheme based on a staggered grid. The discrete equations are second-order accurate and conserve energy, mass and momentum. Advection of scalars ψ is computed by means of the second-order Smolarkiewicz (1984) scheme. Pressure is computed by solving the elliptic equations using FFT and Gaussian elimination for Cartesian grids and a block iteration for terrain following coordinates. For further details see Schumann et al. (1987) and Krettenauer (1991).

2.4 Subgrid-scale (SGS) model

Subsequently, the SGS model is described which we recommend based on previous experiences (Schumann 1991a). It is a first-order closure model of Prandtl-Kolmogorov type. The SGS fluxes are computed using eddy diffusivites K_m for momentum and K_h for heat and other scalars. These diffusivities are computed using the SGS kinetic energy $e \equiv 1/2\overline{u''^2_i}$. The latter is the solution of the following transport equation,

$$\frac{De}{Dt} = -\overline{u''_i u''_j}\frac{\partial \overline{u}_i}{\partial x_j} + \beta g_i \overline{u''_i T''} + \frac{\partial}{\partial x_i}\left[\frac{1}{3}\ell e^{1/2}\frac{\partial e}{\partial x_i}\right] - \varepsilon. \tag{5}$$

The momentum and heat fluxes are computed from

$$\overline{u''_i u''_j} = -K_m\left(\frac{\partial \overline{u}_i}{\partial x_j} + \frac{\partial \overline{u}_j}{\partial x_i}\right) + \frac{\delta_{ij}}{3}\overline{u''^2_k}, \quad \overline{u''_i T''} = -K_h\frac{\partial \overline{T}}{\partial x_i}, \tag{6}$$

and likewise the scalar fluxes $\overline{u''_i \psi''}$. The essential parametrizations concern the dissipation rate ε and the SGS diffusivities,

$$\varepsilon = c_\varepsilon \frac{e^{3/2}}{\ell}, \quad K_m = c_m \ell e^{1/2}, \quad K_h = c_h \frac{\ell e^{1/2}}{1 + 0.3\Delta^2 N^2/e}. \tag{7}$$

Here, the factor containing the Brunt-Väisälä frequency $N = (\beta g \partial T/\partial z)^{1/2}$ is applied only in stable parts of the flow and only for vertical diffusion. It guarantees positive SGS energy e and vanishing vertical diffusion of heat for $\Delta^2 N^2/e \gg 1$. The relevant lengthscale is given by the mean grid spacings,

$$\ell = \min(\Delta, c_\varepsilon z), \quad \Delta = (\Delta x + \Delta y + \Delta z)/3. \tag{8}$$

If ever possible, equidistant and isotropic grid cells are used. The essential model coefficients are the following ones which are computed from inertial subrange theory,

$$c_\varepsilon = \left(\frac{2}{3\alpha}\right)^{3/2} \pi = 0.845, \tag{9}$$

$$c_m = \left(\frac{2}{3\alpha}\right)^{3/2} \frac{1}{\pi} = 0.0856, \quad c_h = \left(\frac{2}{3\alpha}\right)^{1/2} \frac{4}{3\gamma} \frac{1}{\pi} = 0.204, \tag{10}$$

where $\alpha = 1.6$ and $\gamma = 1.34$ are the Kolmogorov and Batchelor coefficients (Schmidt and Schumann, 1989), see also Moeng and Wyngaard (1988).

2.5 Boundary conditions

At the top of the computational domain we set diffusive fluxes to zero and compute the pressure (in its Fourier modes $\hat{p}$) from vertical velocity to allow for upward propagation of gravity waves as proposed by Bougeault (1983) and Klemp and Durran (1983): $\hat{p} = N\rho\hat{w}/k$. At lateral boundaries, periodic conditions are assumed for those applications described in this paper. At the bottom, the surface temperature flux is prescibed,

$$\overline{w''T''}_s = Q_s. \tag{11}$$

Momentum fluxes are determined from the Monin-Obukhov relationships as a function of local friction velocity u_*,

$$\overline{u''_i w''} = -\frac{\overline{u}_i(z)}{U(z)} u_*^2, \quad i = 1, 2, \quad u_* = \kappa\, U(z)\, [\, \ln(z/z_0) - \psi_m(z/L) + \psi_m(z_0/L)]^{-1}, \tag{12}$$

with standard profile functions ψ_m according to Paulson (1970) and Dyer (1974). Here, $L = -u_*^3/(\kappa\beta g Q_s)$ is the local Obukhov scale, $\kappa = 0.41$ is the von Karman constant, and

$$U(z) = (\overline{u}_1^2 + \overline{u}_2^2)^{1/2} + 0.07(\beta g Q_s \Delta z)^{1/3} \tag{13}$$

is the "effective" velocity magnitude at $z = \Delta z/2$. For neutral flows, where $L \to \infty$ and $\psi_m = 0$, this represents the classical logarithmic law of the wall.

3. RESULTS AND PARAMETRIZATIONS FOR THE CBL

3.1 Results from LES

The CBL arises over heated homogeneous surfaces (Stull 1988). Measurements on the turbulence structure in the CBL have been reported by many authors including Kaimal et al. (1976: plumes up to inversion; 1982: spectral characteristics), Caughey and Palmer (1979) and Lenschow et al. (1980: mean turbulence profiles), Hunt, Kaimal and Gaynor (1988: merging plumes), Lenschow and Stephens (1980: updrafts, q-plumes), Greenhut and Khalsa (1987: w-plumes with nonzero thresholds), Young (1988: w-plumes with zero thresholds), and Sorbjan (1990, 1991: similarity function).

LES of the homogeneous CBL have been performed by Deardorff (1972, 1974: CBL for $-z_i/L > 5$), Wyngaard and Brost (1984: top-down and bottom-up diffusion), Moeng (1984, 1986: pseudospectral, dry and stratus), Moeng and Wyngaard (1984, 1986, 1988, 1989, analysis of turbulence models), Nieuwstadt and Brost (1986: decay of convective turbulence), Sykes and Henn (1989: shear effects, confirm Deardorff's results), Mason (1989: SGS-effects, spoke pattern), Nieuwstadt (1990, 1991: review, buoyant stack plumes and

dispersion of a line source), Schmidt and Schumann (1989: spoke pattern, plume dynamics, heat transfer for zero mean wind), Ebert, Schumann and Stull (1989: tracer transport, transilient matrix), Schumann (1989: transport with chemical reactions; 1990: upslope boundary layer), Schumann and Moeng (1991a, b) and Moeng and Schumann (1991: plume structure and related fluxes and budgets), and Shaw et al. (1991: LES of a forest layer below a CBL).

With respect to parametrization, the most important finding is probably that of Deardorff (1970b) who showed that the relevant scales of the CBL are

$$z_i, \quad w_* = (\beta g Q_s z_i)^{1/3}, \quad T_* = Q_s/w_*, \quad t_* = z_i/w_*, \tag{14}$$

for length, velocity, temperature and time, respectively. This result is based on insight Deardorff obtained from his first LES of a CBL. Here, z_i is the depth of the CBL, measured usually as that altitude above ground where the vertical turbulent heat flux reaches a (negative) minimum (alternatively, we will denote this height by H). Typical orders of magnitude are $z_i \cong 1000$ m, $Q_s \cong 0.1$ K ms^{-1}, (corresponding to a heat flux of 100 Wm^{-2}), for which $w_* = 1.5$ ms^{-1}, $T_* = 0.07$ K. Deardorff (1972) deduced from LES the result that the mixed layer of the CBL is controlled solely by buoyant forces if

$$z_i/(-L) = \kappa w_*^3/u_*^3 > 5, \tag{15}$$

where L is the Obukhov lengthscale (negative under unstable conditions), u_* is the mean surface friction velocity, and κ is the von Karman constant. For the given order of magnitude estimates, this means that u_* should stay below 0.6 ms^{-1}, which is quite a large friction velocity. As shown in fig. 1, this CBL condition is typically reached, even for strong mean winds U (say > 10 ms^{-1}) if the layer is thick, the heating strong and the surface roughness height z_0 small.

The turbulent structure of the CBL has clearly been identified from LES. For example, fig. 2 shows the flow field computed by Schmidt and Schumann (1989) using a LES in which 160 x 160 x 48 grid cells where used to resolve the computational domain of 5 x 5 x 1.5 in terms of z_i. These simulations, and also those of Mason (1989), showed more clearly than Deardorff's less resolving earlier simulations a spoke-pattern of convection in the lower quarter of the CBL. From the hubs of the spokes the most energetic updrafts rise of which a few rise up to the inversion and penetrate into the stable troposphere above. These plumes are quasi-steady updrafts persisting over a time of order $2t_*$, but contain also hot bubbles which rise occasionaly within the updrafts even more quickly. Basically the same structure has been found by direct numerical simulations of the CBL for $Re = w_* z_i/\nu = 139$ by Moeng and Rotunno (1990).

The penetrative plumes cause some of the entrainment by which relatively cool air is transported into the warmer (in terms of potential temperature) troposphere above. Moreover, for continuity, warm downdrafts sink from above into the CBL. Both effects together cause a negative entrainment heat flux Q_e at the inversion. As a consequence, the mixed layer gets heated from below by Q_s and from above by Q_e. Also subsidence may contribute considerably to the heat budget (Hoppmann and Roth, 1991). The resultant changes in mean temperature and the rise of the inversion can be parametrized as described in Raynor and Watson (1991). Parametrizations of the surface heat flux at weak

mean winds are deduced from a simple surface layer model in Schumann (1988) and discussed in Schumann and Schmidt (1989) and Schmidt and Schumann (1989).

As shown by fig. 3, the profile of vertical turbulent heat or temperature flux decreases about linearly from its surface value to the entrainment flux. Such a linear profile is necessary to give a uniform vertical divergence of the heat flux which in turn causes a constant heating of the mixed layer within the CBL. The figure shows also that the LES results agree nicely with measurements. In fact, such measurements are difficult and often deviate more from the theoretical linear trend than do the LES results (Sorbjan, 1991). Also the LES results contain statistical uncertainty because of the finite domain size which implies that averages are taken over a finite number of large eddies (updrafts and downdrafts). This statistical uncertainty is indicated by the error bars in fig. 3.

Fig. 4 is taken from a study (Nieuwstadt et al. 1991) in which four LES codes have been compared using rather coarse grids (only 40 x 40 x 40 cells in a domain of size 4 x 4 x 1.5 in units of z_i). The results agree closely with those of the high resolution analysis of Schmidt and Schumann (1989). We see that the scatter between the various LES results is smaller than the scatter of the observational data. Sorbjan (1991) shows similar pictures with more data revealing even larger scatter of the observations. The mean trend of the vertical velocity variance is close to the observations and can be approximated as proposed by Lenschow et al. (1980),

$$\overline{w'^2}/w_*^2 = 1.8(z/z_i)^{2/3}(1 - 0.8z/z_i)^2. \tag{16}$$

See Sorbjan (1990, 1991) and Young (1988) for further parametrizations of this kind. The observations tend, however, to show generally larger horizontal velocity variance $\overline{u'^2}$ than obtained from all the LES. It is assumed that this is caused by deviations from ideal CBL states, e.g. by shear at the inversion or at the surface, surface inhomogeneity (terrain or variable surface heating) or by advection or even by some clouds within the upper CBL.

Fig. 5 shows the mean of the cubed vertical velocity fluctuations and the related skewness, $S = \overline{w'^3}/(\overline{w'^2})^{3/2}$. The vertical velocity cubed describes the turbulent transport of kinetic energy (within the vertical velocity variance). It has to be positive in order to balance for the excess in buoyant energy production near the surface and the excess in energy destruction (both by turbulent dissipation and by the entrainment heat flux) in the upper part of the CBL. In fact, as a rule of thumb, one should expect that this flux increases for larger entrainment flux. This rule is correct as long as the alternative energy flux $\overline{p'w'}/\rho$ does not dominate. See also Moeng and Rotunno (1990) for a discussion of these fluxes as a function of the heat flux profile. The skewness is approximately related to the mean area α_u of updrafts if these are defined as w-plumes, i.e. as those regions where the velocity w' is positive.

The LES result for the updraft area fraction α_u is shown in fig. 6 as computed by Schumann (1989) and by Schumann and Moeng (1991a) in comparison to data by Young (1988). The results differ most strongly in the upper part of the mixed layer where Schumann's LES gives smaller values of α_u. This difference is also found by Nieuwstadt et al. (1989) who found that other LES give results in between those shown in Figs. 6a and 6b.

According to Wyngaard (1987), the relationship between skewness S and area fraction of updrafts α_u is

$$S \cong \frac{1-\alpha_u}{\alpha_u^{1/2}(1-\alpha_u)^{1/2}}, \quad \alpha_u \cong \frac{4+S^2-S\sqrt{4+S^2}}{2(4+S^2)}. \tag{17}$$

However, this relationship underestimates the skewness for given values of $\alpha_u < 0.5$, and underestimates the area fraction of updrafts α_u for given values of S, because it assumes a top-hat velocity field and ignores contributions from skewness within updrafts. For example, it predicts $\alpha_u = 0.28$ for $S = 1$, and $S = 0.41$ for $\alpha_u = 0.4$. The results indicate that a factor of about two should be included for correction, i.e. $S \cong \gamma\overline{S}$, $\alpha_u = 1/2 + (\overline{\alpha}_u - 1/2)/\gamma$, with $\gamma \cong 2$, and $\overline{S}$, $\overline{\alpha}_u$ denoting the values computed from the previous equation.

The variable cross-section of the updrafts and the related skewness profile have strong impact on vertical diffusion. As shown in Fig. 7 (Schumann 1989) and discussed by Wyngaard and Weil (1991) and others, a species introduced through an area source at the layer top and having zero flux through the bottom (i.e., one undergoing "top-down" diffusion) has a well-behaved eddy diffusivity with maximum value of about 0.2. But one introduced at the bottom, with zero flux at the top ("bottom-up" diffusion) has a much different diffusivity profile. It may show a singularity with very large or negative values but is otherwise of order 0.4. The tendency to ill-defined bottom-up diffusion is an effect of counter-gradient diffusion, as explained by Wyngaard and Brost (1984), Schumann (1987) and Holtslag and Moeng (1991). Subsequently, we derive a simple model, which explains the differences in the magnitude of the diffusivites for bottom-up and top-down diffusion.

3.2 Two simple models for bottom-up and top-down diffusion

We consider the simple flow configuration sketched in fig. 8a. The domain of height H and width B is split into four subdomains. The bottom and top domains are of depth $H/2$, the right ones represent the updraft with a width $\alpha_u B$, the left ones the downdraft with width $(1-\alpha_u)B$. We assume a mean steady circulation such that the mean flow rate per unit lenght is wb, where $b = B/2$. This flow rate from subdomain 1 to 2 is the same as that from 2 to 3, 3 to 4, and 4 to 1, because of continuity. We ignore any small-scale turbulent mixing between the subdomains but assume that the single domains become well mixed. The mean concentrations of a species is c_i, $i = 1, 2, 3, 4$, in the four subdomains. The species is emitted from the surface with a uniform flux density U and likewise from the top downwards at rate D. Either U or D is zero. As a consequence, the mean concentration in the whole layer, $\overline{c}$, increases at steady rate by

$$d\overline{c}/dt = (U+D)/H. \tag{18}$$

The mean vertical flux at midlevels in steady state is $(U-D)/2$. Hence, the effective diffusivity K can be estimated from

$$\frac{U-D}{2} = -K\frac{\alpha_u(c_3-c_2)+(1-\alpha_u)(c_4-c_1)}{H/2}. \tag{19}$$

The concentration deviations from the mean $\overline{c}$ satisfy the individual budget equations

$$V_1 dc_1/dt = -wb(c_1 - c_4) + (1 - \alpha_u)BU - V_1 d\bar{c}/dt, \tag{20}$$

$$V_2 dc_2/dt = -wb(c_2 - c_1) + \alpha_u BU - V_2 d\bar{c}/dt, \tag{21}$$

$$V_3 dc_3/dt = -wb(c_3 - c_2) + \alpha_u BD - V_3 d\bar{c}/dt, \tag{22}$$

$$V_4 dc_4/dt = -wb(c_4 - c_3) + (1 - \alpha_u)BD - V_4 d\bar{c}/dt. \tag{23}$$

Here, $V_1 = V_4 = (1 - \alpha_u)BH/2$, $V_2 = V_3 = \alpha_u BH/2$. In steady state, the required concentration differences can easily be found from the above equations:

$$wb(c_3 - c_2) = \alpha_u B(D - U)/2, \quad wb(c_4 - c_1) = (1 - \alpha_u)B(D - U)/2. \tag{24}$$

Hence,

$$K = \frac{(D - U)H}{4[\alpha_u(c_3 - c_2) + (1 - \alpha_u)(c_4 - c_1)]} = \frac{Hw}{4(1 - 2\alpha_u + 2\alpha_u^2)}, \tag{25}$$

independent of D and U. Thus, this model predicts equal diffusivities for bottom-up and top-down diffusion even for $\alpha_u \neq 1/2$. However, the model predicts diffusivities which are up to an factor of two larger for $\alpha_u \ll 1/2$ and for $\alpha_u \gg 1/2$. For $\alpha_u = 1/2$ the model gives $K = wH/2$, i.e. about the right magnitude, $K \cong w_* H/4$, if $w = w_*/2$, which is a reasonable value, see fig. 6.

In order to explain the asymmetry between bottom-up and top-down diffusion, we next consider the alternative simple flow configuration sketched in fig. 8b. The domain of height H and width B is split again into four subdomains but with different topology. The bottom and top domains are of depth $h \ll H$ so that their volume can be ignored in comparison to subdomain 2 which is of width $\alpha_u B$, and represents the updraft region. The downdraft in subdomain 4 is of width $(1 - \alpha_u)B$. Otherwise, the model is as before. Hence, the effective diffusivity can be estimated from

$$\frac{U - D}{2} = -K \frac{c_3 - c_1}{H}. \tag{26}$$

The concentration deviations from the mean $\bar{c}$ satisfy the individual budget equations

$$V_1 dc_1/dt = -wb(c_1 - c_4) + UB - V_1 d\bar{c}/dt, \tag{27}$$

$$V_2 dc_2/dt = -wb(c_2 - c_1) - V_2 d\bar{c}/dt, \tag{28}$$

$$V_3 dc_3/dt = -wb(c_3 - c_2) + DB - V_3 d\bar{c}/dt, \tag{29}$$

$$V_4 dc_4/dt = -wb(c_4 - c_3) - V_4 d\bar{c}/dt. \tag{30}$$

Here, $V_1 = hB \ll V_2$, $V_2 = \alpha_u BH$, $V_3 = hB \ll V_2$, $V_4 = (1 - \alpha_u)BH$. In steady state, the required concentration difference can easily be found from the above equations:

$$wb(c_3 - c_1) = (D - U)B/2 + (V_4 - V_2)(1/2)d\bar{c}/dt = B[(1 - \alpha_u)D - \alpha_u U]. \tag{31}$$

Hence,

$$K = \frac{Hw/2}{1 + (1 - 2\alpha_u)\dfrac{H}{D - U}\dfrac{d\bar{c}}{dt}} = \frac{(D - U)Hw}{4[(1 - \alpha_u)D - \alpha_u U]}. \tag{32}$$

For $D = 0$, $U \neq 0$, we obtain the bottom-up diffusivity, and for $U = 0$, $D \neq 0$, the top-down diffusivity,

$$K_{up} = Hw/(2\alpha_u), \quad K_{down} = Hw/[2(1 - \alpha_u)]. \tag{33}$$

The two values are equal for $\alpha_u = 1/2$ and about $K = wH/2$. This is the same result as in the previous model, see eq. (25), and gives the right magnitude if $w = w_*/2$, which appears not unrealistic, see fig. 6. The ratio of diffusivities is

$$K_{up}/K_{down} = (1 - \alpha_u)/\alpha_u. \tag{34}$$

This result is identical to that given by Wyngaard (1987) but the present model is simpler. The related skewness of vertical velocity is given by eq. (17). Table 1 lists some typical results from these equations. Obviously, the model gives qualitatively the correct trend but the computed asymmetry appears to be too small for the realistic value $\alpha_u = 0.4$. This means that also small-scale motions within the plumes contribute to the asymmetry.

α_u	1/2	0.4	1/3	0.3	1/4	0.2
S	0	0.408	0.707	0.873	1.155	1.5
K_{up}/K_{down}	1	1.5	2	2.33	3	4

Table 1. Influence of updraft area on skewness and diffusivites.

Equation (32) shows that the difference between bottom-up and top-down diffusion originates from the asymmetry of the volumina of those regions into which the upward and the downward diffusing flux is injected, and from the presence of a temporal change in the mean concentrations. The asymmetry of the flow is measured by $\alpha_u = V_2/(V_2 + V_4)$, but lies also in the fact that all fluxes go from the surface through subdomain 1 into 3, without any part mixed directly with subdomain 4, and similar conditions for the top-down diffusing species. The latter point is essential and was not noted before. It appears, however, to be related to the condition of curved mean concentration profiles which were found to be a necessary condition for differences in the diffusivities in a continuum model by Wyngaard and Weil (1991).

Hence, the transport asymmetry is caused in the CBL by the skewed turbulence structure composed of strong updrafts which shrink in mean cross-section with altitude within the mixed layer, and are surrounded by weak and wide downdrafts. It is not sufficient to assume different width for the updraft and downdraft parts rather than the vertical variation in the width of updrafts is important too. The analysis shows further the importance of the time dependence of the concentrations. We expect similar changes in the diffusivities if the concentration changes not because of unsteadiness but because of other source or sink terms as they appear for chemically reacting species. Such effects have been, in fact, observed in LES of the transport of chemically reacting components (Schumann 1989).

4. CONVECTION OVER INHOMOGENEOUS SURFACES

4.1 LES of convection over a surface with variable heat flux

In this section we report on LES of the CBL with variable surface heat flux and variable surface height for zero or very weak mean. The effects of inhomogeneous surface heating on the turbulent CBL over a flat surface has been investigated using LES by several authors. Hadfield (1988) observed a general increase of velocity fluctuations due to an idealized two-dimensional surface heat-flux perturbation. Schmidt (1988) found considerable increase of horizontal velocity fluctuations with increasing inhomogeneity but a small reduction in the vertical velocity component. Graf and Schumann (1991) supported this result from simulations in comparison with field observations including a weak mean wind. Hechtel et al. (1990) simulated an observed case of the CBL with weak mean wind including moisture effects and random surface properties; they found little influence of inhomogeneity on the turbulence statistics. The case of infinitely extended slope layers has been simulated by Schumann (1990). He showed that the turbulent motions dominate relatively to the upslope flow velocity for weak inclination.

As a demonstrative example of the effect of inhomogeneous surface heating, fig. 9 shows results of a LES of a CBL with zero mean wind and with periodically varying surface heating. The simulation parameters are as given in Schmidt and Schumann (1989) except that the surface heat flux varies in a step-wise manner. It amounts to $(2/3)Q$ for $0 \le x \le 2.5\,H$, but to $(4/3)Q$ for $2.5\,H \le x < 5\,H$. Here Q is the mean heat flux and H the depth of the CBL. The resultant mean fields shown in fig. 9 represent averages over all grid points along the y coordinate. We observe a strong coherent circulation pattern. In terms of the convective velocity scale w_*, the maximum updraft/downdraft velocities are $1.02\,/\,-0.4\,w_*$, respectively, the maximum horizontal velocity is $1.32\,w_*$. The updraft deforms the stable layer above the mixed layer only slightly. The resultant heat flux is strongly concentrated and reaches a local maximum of $4.44\,Q$. In spite of the strong local updraft, the mean vertical velocity variance $\overline{w'^2}$, averaged over the x coordinate, is slightly smaller than for the corresponding homogeneous case with constant surface heating; the maximum value of $\overline{w'^2}/w_*^2$ is 0.40 / 0.43 in the inhomogeneous / homogeneous cases, respectively. However, the horizontal velocity variance increases over the inhomogeneous surface; the maximum mean values of $\overline{u'^2}/w_*^2$ occur near the bottom surface and amount to 0.57 / 0.32 in the two cases, respectively.

4.2 LES of convection over wavy surfaces

Field observations of the structure of the atmospheric CBL, by Kaimal et al. (1982), Druilhet et al. (1983), Jochum (1988), and Huynh et al. (1990) found that "gently rolling terrain" affects the turbulence only little. However, the experimental studies did not explain why the effects of terrain appear to be small in most respect.

In a recent study of convection over wavy terrain (Krettenauer 1991), which extended that of Krettenauer and Schumann (1989) to larger Reynolds numbers, and that of Walko et al. (1990) to other parameters, seven cases were treated. The cases are denoted by a string "LddlL", where L stands for LES, dd $\in$ 0, 10, 15, identifies the wave-amplitude δ/H in percent, l $\in$ U, 1, 2, 4, 8, the wavelength λ/H (U for undefined), and L $\in$ 4, 8, denotes the domain size L/H. Fig. 10 depicts the computational domain and the grid on the wavy surface for case L1014. In order to point out that the undulation is strong, we note that the

maximum slope $2\pi\delta/\lambda$ reaches 0.942 with an inclination of 43° for $\delta/H = 0.15$. The surface roughness height (which enters the Monin-Obukhow relationships for momentum and heat transfer) is specified as $z_0 = 10^{-4}H$. As shown in Schmidt and Schumann (1989), the effect of the surface roughness is weak for prescribed heat flux in the convective cases. It is assumed that the CBL is capped by a strong inversion so that vertical fluxes are vanishing at the top of the mixed layer. The numerical scheme uses a grid with $64 \cdot 64 \cdot 16$ grid points for $L = 4\,H$ and $128 \cdot 128 \cdot 16$ grid points for $L = 8\,H$. Hence, the grid cells are close to isotropic with grid spacings of the order $H/16$.

We show first results in terms of mean profiles which are averages at constant transformed coordinates $\eta = const$, see eq. (4), and averaged in addition over the last five time units. Fig. 11 shows a few results from the LES. The undulation effect is largest in the x-component of the velocity variance. The horizontal variances increase with wavelength in x-direction while that in the y-direction gets reduced. This is consistent with an increased excitation of rolls with axis parallel to the surface crests. However, the reduction in v is less systematic than the increase in u variance. The w variance generally changes very little.

Inspection of the instantaneous flow fields shows that the motions are dominated by random motion components which hide the coherent parts induced by the boundary forcing. In order to make the coherent motion parts better visible, we will present results averaged over a finite time period within the final part of the simulation period where the time-average filters out the short-living small-scale random motions and emphasizes the large-scale and long-living parts of the turbulent motions. For this purpose, we average over the time period $30 \leq t/t_* \leq 35$. The limits of this interval are arbitrarily selected; the interval length of 5 convective time units is large enough to detect persistent structures but still small enough to show up turbulent motions. If one would average over an infinite time period, all motions parallel to the crests of the surface waves should average out.

Fig. 12 shows results from case L1018. The wavelength is $\lambda/H = 1$, the amplitude is $\delta/H = 0.1$. We see that the flow is dominated by the few strong updrafts that reach the top boundary. They cause the flow to diverge. Several such divergent flows collide along lines where the fluid sinks back to the mixed layer. The characteristic horizontal scale can be estimated to be 3 to $4\,H$. Although these results are obtained for an undulated lower boundary, the results look isotropic and do not show up this forcing. The vertical cross-section shows clearly that the dominant turbulent scales are larger than the wavelength of the surface.

From horizontal cross-sections for other cases, it has been found that the undulation for $\lambda/H = 2$ causes a flow pattern which is dominated by rolls with horizontal axis. But the axis of these rolls are, surprisingly, not parallel rather than perpendicular to the waves and these rolls get stronger by increasing wave-amplitude. Qualitatively, the same effect was shown by Pal and Kelly (1979) and Krettenauer and Schumann (1989). Shorter surface waves enhance the rolls perpendicular to the crests while longer surface waves drive rolls parallel to the surface wave-crests. Further analysis are reported in Krettenauer and Schumann (1991).

In fig. 13 we investigate the effects of various surface undulations on the time and y-averaged flow fields in a vertical plane. We observe that a regular convection pattern, as to be expected from the forcing by the wavy surface, arises only for $\lambda/H \geq 4$. The averaged motion amplitude is strongest for $\lambda/H = 4$. It increases slightly with increasing wave amplitude.

4.3 A simple model for convection over inhomogeneous surfaces

The behaviour of the CBL over inhomogeneous terrain, as found above, can be explained approximately using a simple model as described in Schumann (1991b). The following description is a highly abridged version of that paper. The model assumes that the flow can be described (in the sense of VLES) by just two grid cells in the vertical and two grid cells in the horizontal per half-wavelength. The resultant flow can be determined quasi analytically. The model includes both the effects from the coherent motion of the most energetic circulation and small-scale turbulent mixing, gives an estimate of the effective small-scale turbulence intensity, and predicts the dynamics of the flow together with the effective diffusivites.

The model considers the turbulent convection in a boundary layer of mean depth H driven by a mean surface temperature flux Q at zero mean wind. The surface is assumed to have a regular wavy form with wavelength λ and amplitude $\delta < H$. The surface heat flux varies also periodically with the same wavelength and amplitude $q < Q$ around the positive mean value Q. We assume that all properties vary piecewise linearly. The resultant mean deviations in the heat fluxes are $\pm q/2$. In the case of fig. 9, $q/Q = 2/3$. The surface is assumed to be rough with roughness height z_0. The top of the boundary layer is assumed to be represented by a very stable inversion such that it can be approximated by a rigid free-slip adiabatic boundary. The fluid is exposed to gravity g. We assume the Boussinesq approximation for a fluid with uniform density ρ, and constant volumetric expansion coefficient β. Because of constant mean surface heating, the volume averaged temperature $\overline{T}$ increases at constant rate

$$d\overline{T}/dt = Q/H. \tag{35}$$

In order to obtain an estimate of the resultant convective (coherent) motions we approximate the flow domain, as sketched in fig. 14, by four subdomains, 1 to 4, each of width $b = \lambda/4$. On average the depth of the subdomains is $h = H/2$. Between the subdomains, we assume a flow with surface averaged velocities u from domain 1 to domain 2, and, for continuity, at the same rate from domain 3 to 4. In the vertical directions the corresponding flow velocities from 2 to 3 and from 4 to 1 have the mean value w. Flow across other boundaries of the subdomains are zero because of symmetry, periodicity and because of top and bottom boundary conditions. Because of continuity,

$$u\,h = w\,b. \tag{36}$$

This equation applies for arbitrary values of $\delta < H$ because the velocities are the Cartesian components and because the domain height is $2h$ at the mid-interface for symmetry. The volume sizes of the four subdomains, per unit length in y direction, are $V_1 = V_4 = b(h + \delta/4)$, $V_2 = V_3 = b(h - \delta/4)$. Let T_i, i = 1, 2, 3, 4, denote the mean local temperature deviations from the (arbitrary) mean temperature $\overline{T}$. We approximate advective

fluxes by "upstream" values, e.g. the flux from volume 1 to volume 2 equals $h\,u\,T_1$. Without loss of generality, this requires $u \geq 0$. Moreover, we apply eq. (36). Then, the heat balance for each of the subdomains results in

$$V_1 dT_1/dt = -(uh + w'b)(T_1 - T_4) - u'h(T_1 - T_2) + (Q - q/2)b - V_1 d\overline{T}/dt, \tag{37}$$

and similar equations for the other subdomains (Schumann 1991b). Here, u' and w' are effective turbulence velocities such that, e.g., $w'(T_1 - T_4) = -K_v(T_4 - T_1)/h$, describes the turbulent flux density between volumes, e.g. from 1 into 4. They are related to horizontal and vertical diffusivities,

$$K_h = u'b \text{ and } K_v = w'h, \tag{38}$$

respectively.

The horizontal momentum balance is set up for a control volume of size $V_u = b\,h$ enclosing either the lower or the upper lateral interfaces between volumes 1 and 2 and between 3 and 4. The shear stress at the bottom surface is denoted by $-u_*^2$ as a function of the friction velocity u_*. To first order in geometrical terms, the balances are

$$V_u du/dt = p_3(h - \delta/4) - p_4(h + \delta/4) - 2w'ub + (p_1 + p_2 + p_3 + p_4)\delta/8. \tag{39}$$

for the upper volume, and similarly for the lower volume. Here p_i is the mean pressure (per unit mass) in the i-th control volume. Similarly, the vertical momentum balance is formulated for the two control volumina enclosing the interface between subdomains 2 and 3 and 4 and 1.

To close the set of equations, we have to specify the turbulent diffusivities K_h, K_v, and the surface friction velocity u_*. The latter is related to the horizontal flow velocity u according to the Monin-Obukhov relationships, following Paulson (1970) and Dyer (1974), as used in the LES boundary conditions. They are evaluated for $z = h/2$.

The turbulent diffusivities are roughly approximated by

$$K_h = 3\alpha v'h, \quad K_v = \alpha v'h, \text{ so that } u' = 3\alpha v'h/b, \quad w' = \alpha v'. \tag{40}$$

Here, $\alpha \cong 0.079$ and $K_h/K_v \cong 3$ are empirical parameters.

The effective turbulence velocity scale v' is determined from an energy balance as follows. The total kinetic energy $E_{tot} = E + e$, averaged over the whole domain, is composed of the energy $E = \gamma(u^2 + w^2)/2$ of the coherent motion part plus $e = 3v'^2/2$, the turbulent motion part. The factor γ measures the ratio between the averaged energy of the coherent motion and its maximum value. For a linear variation of the velocities within the four subdomains, as it is consistent with the present model concept, we have $\gamma = 1/3$. The total energy satisfies

$$d(E + e)/dt = \beta gQ/2 - \varepsilon, \tag{41}$$

where the source term describes the energy production due to buoyancy and ε is the viscous dissipation rate. The factor 1/2 enters the buoyant part because the mean heat flux decreases from its surface value to zero at the top and equals $Q/2$ on average. Shear contributions from the coherent motions are irrelevant in this sum, because shear pro-

duction of turbulent motions equals shear energy loss of coherent motions. Also diffusion and pressure contributions vanish because they are zero in the volume mean for the given boundary conditions. The energy of the coherent motion part satisfies

$$\frac{d}{dt}E = \gamma\left(u\frac{du}{dt} + w\frac{dw}{dt}\right) = \gamma u\frac{du}{dt}\left(1 + h^2/b^2\right), \tag{42}$$

where the last relation comes from continuity. The difference of eqs. (41) and (42), normalized by w_* gives

$$\frac{H}{w_*^3}\frac{d}{dt}e = \frac{1}{2} - \frac{H\varepsilon}{w_*^3} - \gamma\frac{u}{w_*}\frac{H}{w_*^2}\frac{du}{dt}\left(1 + 4H^2/\lambda^2\right). \tag{43}$$

The acceleration term du/dt is given by eq. (39), or finally by eq. (47) below. The dissipation rate ε is commonly related to the turbulence velocities by

$$\varepsilon = e^{3/2}/L_\varepsilon = (3v'^2/2)^{3/2}/L_\varepsilon, \tag{44}$$

where L_ε is the dissipation lengthscale. For the homogeneous case and vanishing coherent motions, e comprises the total kinetic energy. For this case, Krettenauer and Schumann (1991) show that $L_\varepsilon \cong 0.93\,H$. For a CBL topped by a finite inversion this value is little smaller and about $0.8\,H$ (Schumann, 1991a). If the coherent motions are non-zero, the lengthscale is smaller because it measures the size of the turbulent parts only. Hunt et al. (1989) proposed to relate L_ε to the mean shear. In rough agreement with their proposal, we set

$$L_\varepsilon = 0.93\left[H^{-1} + \sigma\frac{2}{w_*}\left\{(u/h)^2 + (w/b)^2\right\}^{1/2}\right]^{-1}. \tag{45}$$

Here, $2u/h$ and $2w/b$ are the effective shear rates in the horizontal and vertical directions. The coefficient σ is to be adjusted empirically. We will present results for $\sigma = 1$, but the results don't change significantly if we vary σ between 0.5 and 2. These approximations allow us to compute v' from eq. (43) for steady state, i.e. for $de/dt = 0$,

$$\frac{v'^3}{w_*^3} = (2/3)^{3/2}\frac{L_\varepsilon}{H}\left\{\frac{1}{2} - \gamma\frac{u}{w_*}\frac{H}{w_*^2}\frac{du}{dt}\left(1 + 4H^2/\lambda^2\right)\right\}. \tag{46}$$

From the solution v', we can now determine the diffusivities as a function of the turbulence intensity, using eq. (40). For $u = 0$, eq. (46) predicts realistically a rms value $v' = [(2/3)^{3/2}0.93/2]^{1/3}w_* \cong 0.633\,w_*$. The corresponding total energy is $E_{tot} = 0.6\,w_*^2$.

4.4 Solutions of the simple model for convection over inhomogeneous surfaces

For steady state, the model equations can be solved analytically to determine the pressure and the temperature fields. From this one finds an equation for the velocity,

$$\frac{H}{w_*^2}\frac{du}{dt} = -4\left(\frac{8u'}{w_*}H^3/\lambda^3 + \frac{w'}{w_*}\right)\frac{u}{w_*} - u_*^2/w_*^2 + \frac{w_*\{2w + (w + 2w')(\delta/H + q/Q) + [4u' + u(2 - \delta/H - q/Q)]\delta/\lambda\}}{8[w(u + u') + w'(u + 2u')]}. \tag{47}$$

For steady state ($du/dt = 0$), the solution u/w_* of this equation can be determined iteratively. Analytic solutions exist for limiting cases, which we give below for $v' = w_*$. For $\lambda/H \to \infty$, $u'/w_* \to 0$, compare eq. (40), and therefore

$$\frac{u}{w_*} = \frac{1}{2}\sqrt{\frac{q/Q + \delta/H}{4w'/w_* + C_d u_*/w_*}}, \quad \frac{w}{w_*} \to 0, \quad C_d \equiv \frac{u_*}{u}. \tag{48}$$

In this limit, variations by δ/H and q/Q have equivalent effects. One obtains a finite coherent circulation which magnitude depends strongly on the vertical turbulence velocity w' and also on the friction velocity u_*. Obviously, the smaller the turbulence velocity scales are the stronger is the large-scale convection. Since $C_d \ll 1$, surface friction will in general be less important than the convective turbulence in limiting the coherent motions.

In the other extreme, for very short wavelengths, $\lambda/H \ll 1$, we obtain $u \ll u'$, $w \ll w'$, $C_d \to 0$, and

$$\frac{u}{w_*} = \frac{1}{18432}\frac{1}{\alpha^2}\frac{\lambda^5}{H^5}\left(\delta/H + q/Q + 24\frac{H}{\lambda}\frac{\delta}{\lambda}\right). \tag{49}$$

Here, the terms containing δ vanish over smooth terrain where δ/H goes to zero faster than $(\lambda/H)^2$. The result suggests zero motions over homogeneous terrain and a strong dependence on α, i.e. on turbulent diffusion. The results for the limiting cases of large and small wavelengths together show the existence of a wavelength λ_{max} with maximum coherent motion.

For a wavelength of order 4 H the model solutions suggest that $u' \ll u$ and $w' \ll u$. For such conditions, eq. (47) reduces to an explicit expression for the coherent flow amplitude,

$$\frac{u}{w_*} = \sqrt{\frac{1 + \delta/H + q/(2Q) - (\delta/H + q/Q)\delta/(4H)}{19\alpha + 4C_d u_*/w_*}}. \tag{50}$$

It shows that the surface friction plays the smaller role in comparison to the convective turbulence in limiting the coherent motions. Moreover, we note a nonlinear interaction of undulation and variable heat flux which tends to reduce the convection for large values of δ/H. Since $C_d \ll 1$, we find for $\lambda = 4H$ and for small inhomogeneities the simple result

$$\frac{u}{w_*} \cong A\left[1 + \frac{\delta}{2H} + \frac{q}{4Q}\right], \quad w = \frac{u}{2}. \tag{51}$$

Here, $A \cong 1.0$ for $\alpha = 0.05$, and $A \cong 0.7$ for $\alpha = 0.1$.

Fig. 15 shows the resultant turbulence intensities in terms of total kinetic energy and in terms of the individual components, for $\delta/H = 0.1$, $q = 0$. It should be noted that these results depend quite strongly on the model parameters, in particular on α and γ. We see that v'^2, which corresponds to the total variance in the y direction, decreases with λ/H up to a broad minimum near λ/H of order five. The vertical velocity variance, computed as the sum of coherent and turbulent motions, shows a non-monotonic behaviour but decreases and reaches v'^2 for large wavelengths. Only the horizontal velocity variance shows a significant increase at $\lambda/H > 2$. However, this increase is not strong enough to prevent a slight reduction in total kinetic energy. The coherent motion amplitude stays

finite for very large wavelengths because of the finite terrain undulation. Therefore, for $\lambda/H \to \infty$, all energy components are smaller than for $\lambda = 0$. The analysis suggests that the relevant tubulent scale decreases with increasing u_*/w_*, at least for small values of this ratio.

Fig. 16 shows that the coherent flow part achieves a maximum at about 2 to 3 H with respect to the vertical velocity component. The horizontal one is maximum near 4 H. The critical wavelength increases slightly for increasing inhomogeneity parameters. The effect from surface undulation is little larger than from variation of the heat flux but approximately the same for $\delta/H = q/(2Q)$. The numerical results show the strong increase for small λ/H, see eq. (49). We see that both inhomogeneity parameters increase the coherent circulation, but the circulation is quite large already for a homogeneous surface. Further parameter studies have shown a very weak sensitivity to the surface roughness height; its effect is less than 3 % for $z_0/H < 10^{-4}$.

As shown by the LES results and observations, the characteristic distance between updrafts and the wavelength of w-spectra is of order 2 to 4H for homogeneous surfaces. Also, the maximum root-mean-square value of the horizontal velocity fluctuations and the maximum value of u in conditional plume averages is of order 0.7w_*. Moreover, we found a maximum response to wavy terrain for $\lambda \cong 4H$. These findings are in rough agreement with the prediction of the model.

The flow results can be used to evaluate the vertical diffusivity for the heat flux K_v. The result is

$$K_V = \frac{H[w(u+u') + w'(u+2u')]}{4u' + u(2 - \delta/H - q/Q)} . \tag{52}$$

For $u' \ll u$,

$$K_V = \frac{(w+w')H}{2 - \delta/H - q/Q} . \tag{53}$$

Hence, K_v increases with increasing amplitude of the coherent motions. We expect a maximum for $\lambda/H \cong 3$, where the vertical velocity achieves its maximum. For larger wavelengths, the diffusivity decreases. This is reasonable because any heat added to the lower subdomain is first transported with the mean circulation horizontally before it eventually is carried upwards. The larger the horizontal circulation wavelength, the slower will be the vertical mixing. We further observe an increase of vertical diffusivity with increasing inhomogeneity. This comes from increase in vertical velocity which enters the above expression explicitly and also by reducing the vertical temperature differences; the latter causes the factor in the denominator. For $\lambda/H = 4$, we may apply eq. (51) to estimate $w = uh/b$ so that

$$K_V \cong w_* H \frac{A}{4} \left(1 + \frac{\delta}{H} + \frac{3}{4}\frac{q}{Q}\right). \tag{54}$$

Fig. 17 depicts the dependence of K_v, eq. (52), on λ/H and on the inhomogeneity parameters. As to be expected from the above analysis, the diffusivity is small for $\lambda/H = 0$, and

maximum near $\lambda/H \cong 3$. For very large wavelengths, it returns to the value for $\lambda/H = 0$ because of vanishing vertical mean velocity. This result suggests a strong impact of inhomogeneities on vertical mixing. This is true with respect to internal mixing. However, the mixing from the surface into the CBL is controlled by small-scale turbulence which is much less affected by the coherent motions.

The effective horizontal diffusivity which controls the heat flux, induced by the differential heating q between the left subdomains (1 and 4) and the right ones (2 and 3), is

$$K_H = \frac{\lambda}{4} \frac{w(u+u') + w'(u+2u')}{w+2w'}. \tag{55}$$

Note that this diffusivity depends on the inhomogeneity parameters only indirectly by virtue of u and w. For very small wavelength or vanishing coherent motions, it equals $K_H = K_h = bu' = 3\alpha v' H/2$. For larger wavelength, however, its value increases up to infinity as $K_H \to \lambda u/8$. For $u' \ll u$, $w' \ll w$, $K_H = \lambda u/4$. The ratio of horizontal to vertical diffusivities is $K_H/K_V \cong \lambda^2/(4H^2)$ for such conditions and small inhomogeneity. For $\lambda = 4H$ we obtain $K_H \cong 4K_V$ and

$$K_H \cong w_* HA[1 + \delta/(2H) + q/(4Q)]. \tag{56}$$

Finally, we compute the diffusivities for vertical transport of a scalar which is emitted with mean flux C and horizontal variability c, as corresponding to Q and q. For bottom-up diffusion, i.e. for given surface fluxes and zero fluxes at the top of the boundary layer, the budget equations for the species concentrations c_i in the four domains are formally the same as those for the temperatures T_i. We obtain

$$K_{up} = \frac{H[w(u+u') + w'(u+2u')]}{4u' + u(2 - \delta/H - c/C)}. \tag{57}$$

Note the formal similarity to K_V, eq. (52), as expected. For $u' \ll u$, $w' \ll w$, and $\lambda/H = 4$, using eq. (51), this gives

$$K_{up} \cong w_* H \frac{A}{4}\left(1 + \frac{\delta}{H} + \frac{q}{4Q} + \frac{c}{2C}\right). \tag{58}$$

For the top-down diffusion case, we assume that the fluxes are imposed at the top boundary, simulating entrainment flux from above the inversion. The flux C is taken positively downwards; the variation c is positive if the flux into subdomain 3 is larger than into subdomain 4, depicted in fig. 14. The result is

$$K_{down} = H \frac{w(u+u') + w'(u+2u')}{4u' + u(2 + \delta/H + c/C)}. \tag{59}$$

For $u' \ll u$, $w' \ll w$, and $\lambda = 4H$, one obtains

$$K_{down} \cong w_* H \frac{A}{4}\left(1 + \frac{q}{4Q} - \frac{c}{2C}\right). \tag{60}$$

We see that the bottom-up diffusivity is larger than the top-down diffusivity over undulated terrain. This is a consequence of the asymmetry of the flow structure. For bottom-up dif-

fusion the species is transported first with the shorter updraft while for top-down diffusion the species is transported first with the longer downdraft. It is interesting to see that an asymmetry of geometrical nature has similar effects as an asymmetry of dynamical nature. This effect was not noted before. The bottom-up diffusivity is also larger than its top-down counterpart if $c > 0$. This is caused by the fact that the extra flux c is added into the upward branch of the circulation from below (subdomain 2) but into the horizontal branch from above (subdomain 3). This topological asymmetry drops if the sign of c is changed at one of the boundaries. For $\delta = c = 0$, i.e. for homogeneous surfaces, the present model gives equal values for both kinds of diffusion, and basically the same as eq. (25) for $\alpha_u = 1/2$. This is, as we have seen, not realistic, but a consequence of the symmetric flow structure which is assumed in this model.

5. CONCLUSIONS AND OUTLOOK

It has been shown that LES provides reliable data on the structure of the CBL. We have deduced various simple models to expain the differences between vertical and horizontal diffusivity and their dependence on the horizontal scale of the convective circulation. We showed that several conditions must come together to explain the differences between bottom-up and top-down diffusion. These include the nonstationarity (or other sink terms), the skewness, and the vertical variability of the updraft area. Wavy terrain with moderate amplitude ($\delta < 0.15\, z_i$) has generally small impact but has strongest effect for $\lambda \cong 4\, z_i$. This can be explained quasi analytically.

Certainly, the potential of LES studies is very large, in particular for cloudy cases and stratified turbulence. In an ongoing study (Dörnbrack et al. 1991) we investigate the effects of flow over wavy terrain, both with and without a troposphere of finite stability. Here an important question is the effect of a turbulent boundary layer over wavy terrain on the gravity-wave momentum transport within the troposphere. Other ongoing activities concern the LES of dispersion in homogenous stratified and sheared turbulence (Kaltenbach et al., 1991) and the wave breaking and related dispersion in a stable troposphere due to decreasing mean density and shear.

The success of the very simple models, which just use two grid cells in the vertical, suggests that refinements in resolution near the surface is often unnecessary and a waste of computer time. In contrary, one should try to get comparable resolution in horizontal as in vertical directions. With two grid cells per mean boundary layer thickness in all spatial coordinates, VLES may become possible in the not too far future even for numerical weather predictions.

6. REFERENCES

Aldama, A.A., 1990: *Filtering techniques for turbulent flow simulation.* Lecture Notes in Engineering, Vol. 56, Springer-V., Berlin.

Bougeault, P., 1983: A non-reflective upper boundary condition for limited-height hydrostatic models. *Mon. Wea. Rev.* **111**, 420-429.

Caughey, S.J. and S.G. Palmer, 1979: Some aspects of the turbulent structure through the depth of the convective boundary layer. *Q. J. R. Met. Soc.* **105**, 811-827.

Clark, T., 1977: A small-scale dynamical model using a terrain-following coordinate transformation. *J. Comput. Phys.* **24**, 186-215.

Deardorff, J.W., 1970a: A numerical study of three-dimensional turbulent channel flow at large Reynolds number. *J. Fluid Mech.* **41**, 453-480.

Deardorff, J.W., 1970b: Convective velocity and temperature scales for the unstable planetary boundary layer and for Rayleigh convection. *J. Atmos. Sci.* **27**, 1211-1213.

Deardorff, J.W., 1971: On the magnitude of the subgrid scale eddy coefficient. *J. Comput. Phys.* **7**, 120-133.

Deardorff, J.W., 1972: Numerical investigation of neutral and unstable planetary boundary layers. *J. Atmos. Sci.* **29**, 91-115.

Deardorff, J.W., 1973: The use of subgrid transport equations in a three-dimensional model of atmospheric turbulence. *J. Fluids Eng.*, **95**, 429-438.

Deardorff, J.W., 1974: Three-dimensional numerical study of the height and mean structure of a heated planetary boundary layer. *Bound. Layer Meteor.* **7**, 81-106.

Deardorff, J.W., 1980: Stratocumulus-capped mixed layers derived from a three-dimensional model. *Boundary-Layer Meteor.* **18**, 495-527.

Dörnbrack, A., K. Krettenauer and U. Schumann, 1991: Numerical simulation of turbulent convective shear flows over wavy terrain. *Proc. 8th Turbulent Shear Flow Symp.*, Munich, 9-11 Sept. 1991, p. 19.5.1 - 19.5.6.

Druilhet, A., J. Noilhan, B. Benech, G. Dubosclard, D. Guedalia and J. Frangi, 1983: Étude expérimentale de la couche limite au-dessus d'un relief modéré proche d'une chaîne de montagne. *Bound.-Layer Meteor.* **25**, 3-16.

Dyer, A.J., 1974: A review of flux-profile relationships. *Bound.-Layer Meteor.* **7**, 363-372.

Ebert, E.E., U. Schumann and R.B. Stull, 1989: Nonlocal turbulent mixing in the convective boundary layer evaluated from large-eddy simulation. *J. Atmos. Sci.* **46**, 2178-2207.

Ferziger, J.H., 1977: Large eddy simulations of turbulent flows. *AIAA J.* **15**, 1261-1267.

Ferziger, J.H., 1987: Simulation of incompressible turbulent flows. *J. Comput. Phys.* **69**, 1-48.

Friedrich, R. and M. Arnal, 1990: Analysing turbulent backward-facing step flow with the lowpass-filtered Navier-Stokes equations. *J. Wind Engrg. Ind. Aerodyn.*, **35**, 101-128.

Germano, M., 1991: An algebraic property of the turbulent stress and its possible use in subgrid modeling. *Proc. 8th Turbulent Shear Flow Symp.*, Munich, 9-11 Sept. 1991, p. 19.1.1 - 19.1.6.

Gerz, T., U. Schumann and S.E. Elghobashi, 1989: Direct numerical simulation of stratified homogeneous turbulent shear flows. *J. Fluid Mech.* **200**, 563-594.

Graf, J. and U. Schumann, 1991: Simulation der konvektiven Grenzschicht im Vergleich mit Flugzeugmessungen beim LOTREX-Experiment. *Meteorol. Rdsch.*, **43**, 140-148.

Greenhut, G.K. and S.J.S. Khalsa, 1987: Convective elements in the marine atmospheric boundary layer. Part I: Conditional sampling statistics. *J. Clim. Appl. Meteor.* **26**, 813-822.

Grötzbach, G., 1986: Direct numerical and large eddy simulation of turbulent channel flows. In: N. P. Cheremisinoff (ed.): *Encyclopedia of Fluid Mechanics*, Vol. 6, Gulf Publ. Co., Houston, Texas, USA, 1337-1391.

Hadfield, M.G., 1988: The response of the atmospheric convective boundary layer to surface inhomogeneities. Colorado State University, Atmos. Sci. Paper No. 433.

Haren, L. van and F.T.M. Nieuwstadt, 1989: The behaviour of passive and buoyant plumes in a convective boundary layer, as simulated with a large eddy model. *J. Appl. Meteor.* **28**, 818-830.

Hechtel, L. M., C.-H. Moeng and R.B. Stull, 1990: The effects of nonhomogeneous surface fluxes on the convective boundary layer: A case study using large-eddy simulation. *J. Atmos. Sci.* **47**, 1721-1741.

Holtslag, A.A.M. and C.-H. Moeng, 1991: On eddy diffusivity and counter-gradient transport in the convective atmospheric boundary layer. *J. Atmos. Sci.*, in print.

Hoppmann, U. and R. Roth, 1991: Der Einfluß großräumiger Absinkbewegungen auf den Energiehaushalt einer konvektiven Grenzschicht unterhalb einer Inversion. *Meteorol. Rdsch.*, **43**, 118-122.

Hunt, J.C.R., J.C. Kaimal and J.E. Gaynor, 1988: Eddy structure in the convective boundary layer - new measurements and new concepts. *Q. J. R. Meteorol. Soc.* **114**, 827-858.

Hunt, J.C.R., P. Moin, R.D. Moser, P. Spalart, M.N. Mansour, J.C. Kaimal and E. Gaynor, 1989: Cross correlation and length scales in turbulent flows near surface. In H.-H. Fernholz and H. E. Fiedler (Ed.): *Advances in Turbulence 2*, p. 128-134, Springer, Berlin.

Huynh, B.P., C.E. Coulman and T.R. Turner, 1990: Some turbulence characteristics of convectively mixed layers over rugged and homogeneous terrain. *Bound.-Layer Meteor.* **51**, 229-254.

Jochum, A., 1988: Turbulent transport in the convective boundary layer over complex terrain. *Proc. Eighth Symposium on Turbulence and Diffusion*, San Diego, Americ. Meteorol. Soc., Boston, Mass., p. 417-420

Kaimal, J.C., J.C. Wyngaard, D.A. Haugen, O.R. Coté, Y. Izumi, S.J. Caughey and C.J. Readings, 1976: Turbulence structure in the convective boundary layer. *J. Atmos. Sci.* **33**, 2152-2169.

Kaimal, J.C., R.A. Eversole, D.H. Lenschow, B.B. Stankov, P.H. Kahn and J.A. Businger, 1982: Spectral characteristics of the convective boundary layer over uneven terrain. *J. Atmos. Sci.* **39**, 1098-1114.

Kaltenbach, H.-J., T. Gerz. and U. Schumann, 1991: Comparison of direct and large-eddy simulation of turbulent scalar transport in stably stratified shear flows. *Proc. 8th Turbulent Shear Flow Symp.*, Munich, 9-11 Sept. 1991, p. 12.4.1 - 12.4.6.

Klemp, J.B. and D.R. Durran, 1983: An upper boundary condition permitting internal gravity wave radiation in numerical mesoscale models. *Mon. Wea. Rev.* **111**, 430-444.

Krettenauer, K., 1991: Numerische Simulation turbulenter Konvektion über gewellten Flächen. Dissertation, report DLR-FB 91-12, DLR Oberpfaffenhofen, 162 pp.

Krettenauer, K. and U. Schumann, 1989: Direct numerical simulation of thermal convection over a wavy surface. *Meteorol. Atmos. Phys.* **41**, 165-179.

Krettenauer, K. and U. Schumann, 1991: Numerical simulation of turbulent convection over wavy terrain. Submitted to *J. Fluid Mech.*

Lenschow, D.H. and P.L. Stephens, 1980: The role of thermals in the convective boundary layer. *Bound.-Layer Meteor.* **19**, 509-532.

Lenschow, D.H., J.C. Wyngaard and W.T. Pennell, 1980: Mean-field and second-moment budgets in a baroclinic, convective boundary layer. *J. Atmos. Sci.* **37**, 1313-1326.

Lenschow, D.H. and B.B. Stankov, 1986: Length scales in the convective boundary layer. J. Atmos. Sci. **43**, 1198-1209.

Leonard, A., 1974: Energy cascade in large-eddy simulations of turbulent fluid flows. *Adv. Geophys.* **18A**, 237-248.

Lilly, D.K., 1962: On the numerical simulation of buoyant convection. *Tellus* **14**, 148-172.

Lilly, D.K., 1965: On the computational stability of numerical solutions of time-dependent non-linear geophysical fluid dynamics problems. *Monthly Wea. Rev.* **93** 11-26.

Lilly, D.K., 1967: The representation of small-scale turbulence in numerical simulation experiments. In: H. H. Goldstine (ed.): *Proc. of the IBM Sci. Comp. Symp. on Env. Sci.*, Nov. 14-16, 1966, New York, IBM-Form No. 320-1951, pp. 195-210.

Mason, P.J., 1989: Large eddy simulation of the convective atmospheric boundary layer. *J. Atmos. Sci.* **46**, 1492-1516.

Mason, P.J. and N.S. Callen, 1986: On the magnitude of the subgrid-scale eddy coefficient in large-eddy simulations of turbulent channel flow. *J. Fluid Mech.* **162**, 439-462.

Mason, P.J. and S.H. Derbyshire, 1990: Large-eddy simulation of the stably-stratified atmospheric boundary layer. *Bound.-Layer Meteor.* **53**, 117-162.

Mason, P.J. and D.J. Thomson, 1991: Stochastic backscatter in the near wall region of large-eddy simulations. *Proc. 8th Turbulent Shear Flow Symp.*, Munich, 9-11 Sept. 1991, p. 19.2.1 - 19.2.5.

Moeng, C.-H., 1984: A large-eddy-simulation model for the study of planetary boundary-layer turbulence. *J. Atmos. Sci.* **41**, 2052-2062.

Moeng, C.-H., 1986: Large-eddy simulation model of a stratus-topped boundary layer. Part I: Structure and budgets. *J. Atmos. Sci.* **43**, 2886-2900.

Moeng, C.-H. and J.C. Wyngaard, 1984: Statistics of conservative scalars in the convective boundary layer. *J. Atmos. Sci.* **41**, 3161-3169.

Moeng, C.-H. and J.C. Wyngaard, 1986: An analysis of closures for pressure-scalar covariances in the convective boundary layer. *J. Atmos. Sci.* **43**, 2499-2513.

Moeng, C.-H. and J.C. Wyngaard, 1988: Spectral analysis of large-eddy simulations of the conservative boundary layer. *J. Atmos. Sci.* **45**, 3573-3587.

Moeng, C.-H. and J.C. Wyngaard, 1989: Evaluation of turbulent transport and dissipation closures in second-order modeling. *J. Atmos. Sci.* **46**, 2311-2330.

Moeng, C.-H. and R. Rotunno, 1990: Vertical-velocity skewness in the buoyancy-driven boundary layer. *J. Atmos. Sci.* **47**, 1149-1162.

Moeng, C.-H., and U. Schumann, 1991: Composite structure of plumes in stratus-topped boundary layers. *J. Atmos. Sci.* **48**, in print.

Nieuwstadt, F.T.M., 1990: Direct and large-eddy simulation of free convection. *Proc. 9th Intern. Heat Transfer Conference*, Jerusalem, 19-24 August, Americ. Soc. Mech. Engrg., Vol. I, pp. 37-47.

Nieuwstadt, F.T.M., 1991: A large-eddy simulation of a line source in a convective atmospheric boundary layer. Part I: Dispersion characteristics. *Atmos. Environm.*, to appear.

Nieuwstadt, F.T.M. and R.A. Brost, 1986: Decay of convective turbulence. *J. Atmos. Sci.* **43**, 532-546.

Nieuwstadt, F.T.M., P.J. Mason, C.-H. Moeng and U. Schumann, 1991: Large-eddy simulation of the convective boundary layer: A comparison of four computer codes. *Proc. 8th Turbulent Shear Flow Symp.*, Munich, 9-11 Sept. 1991, p. 1.4.1 - 1.4.6.

Pal, D. and R.E. Kelly, 1979: Three-dimensional thermal convection produced by two-dimensional thermal forcing. Amer. Soc. of Mech. Engineers, paper ASME 79-HT-109, 8 pp.

Paulson, C.A., 1970: The mathematical representation of wind speed and temperature profiles in the unstable atmospheric surface layer. *J. Appl. Meteor.* **9**, 857-861.

Piacsek, S.A. and G.P. Williams, 1970: Conservation properties of convection difference schemes. *J. Comput. Phys.* **6**, 392-405.

Piomelli, U., J. Ferziger, P. Moin and J. Kim, 1989: New approximate boundary conditions for large-eddy simulations of wall-bounded flow. *Phys. Fluids* **A1**, 1061-1068.

Rayner, K.N. and I.D. Watson, 1991: Operational prediction of daytime mixed layer heights for dispersion modelling. *Atmos. Environm.* **25A**, 1427-1436.

Reynolds, W. C., 1990: The potential and limitations of direct and large eddy simulations. In J.L. Lumley (Ed.): *Whither Turbulence? Turbulence at the Crossroads*. Spinger, Berlin, p. 313-343.

Rogallo, R.S. and P. Moin, 1984: Numerical simulation of turbulent flows. *Annu. Rev. Fluid Mech.* **16**, 99-137.

Schemm, C.E. and F.B. Lipps, 1976: Some results of a simplified three-dimensional numerical model of atmospheric turbulence. *J. Atmos. Sci.* **33**, 1021-1041.

Schmidt, H., 1988: Grobstruktur-Simulation konvektiver Grenzschichten. Thesis, Univ. Munich, report DFVLR-FB 88-30, DLR Oberpfaffenhofen, 143 pp.

Schmidt, H. and U. Schumann, 1989: Coherent structure of the convective boundary layer deduced from large-eddy simulation. *J. Fluid Mech.* **200**, 511-562.

Schumann, U., 1975: Subgrid scale model for finite difference simulations of turbulent flows in plane channels and annuli. *J. Comput. Phys.* **18**, 376-404.

Schumann, U., 1977: Realizability of Reynolds-stress turbulence models. *Phys. Fluids* **20**, 721-725.

Schumann, U., 1985: Conservation properties of finite difference Euler equations. *ZAMM* **65**, T 243-245.

Schumann, U., 1980: Fast elliptic solvers and their application in fluid dynamics. W. Kollmann, ed.: *Computational Fluid Dynamics*, Hemisphere, Washington (1980), 401-430.

Schumann, U., 1987: The countergradient heat flux in stratified turbulent flows. *Nucl. Engrg. Des.* **100**, 255-262.

Schumann, U., 1988: Minimum friction velocity and heat transfer in the rough surface layer of a convective boundary layer. *Bound.-Layer Meteor.* **44**, 311-326.

Schumann, U., 1989: Large-eddy simulation of turbulent diffusion with chemical reactions in the convective boundary layer. *Atmos. Environ.* **23**, 1713-1727.

Schumann, U., 1990: Large-eddy simulation of the upslope boundary layer. *Q. J. R. Met. Soc.* **116**, 637-670.

Schumann, U., 1991a: Subgrid length-scales for large-eddy simulation of stratified turbulence. *Theoret. Comput. Fluid Dynamics* **2**, 98-119.

Schumann, U., 1991b: A simple model of the convective boundary layer over wavy terrain with variable heat flux. Submitted to *Beitr. Phys. Atmosph.*

Schumann, U. and R. Friedrich, 1987: On direct and large eddy simulation of turbulence. In G. Comte-Bellot and J. Mathieu, ed.: *Advances in Turbulence*, Springer, Berlin, 88-104.

Schumann, U., T. Hauf, H. Höller, H. Schmidt and H. Volkert, 1987: A mesoscale model for the simulation of turbulence, clouds and flow over mountains: Formulation and validation examples. *Beitr. Phys. Atmosph.* **60**, 413-446.

Schumann, U. and R.A. Sweet, 1988: Fast Fourier transforms for direct solution of Poisson's equation with staggered boundary conditions. *J. Comput. Phys.* **75**, 123-137

Schumann, U. and H. Schmidt, 1989: Heat transfer by thermals in the convective boundary layer. H.-H. Fernholz, H.E. Fiedler, ed.: *Advances in Turbulence 2*, Springer-V., p. 210-215.

Schumann, U. and H. Volkert, 1984: Three-dimensional mass- and momentum-consistent Helmholtz-equation in terrain-following coordinates. In: W. Hackbusch (Ed.), *Notes on Numer. Fluid Mech.* Vol. 10, Vieweg, Braunschweig, 109-131.

Schumann, U. and C.-H. Moeng, 1991a: Plume fluxes in clear and cloudy convective boundary layers. *J. Atmos. Sci.* **48**, 1746-1757.

Schumann, U. and C.-H. Moeng, 1991b: Plume budgets in clear and cloudy convective boundary layers. *J. Atmos. Sci.* **48**, 1758-1770.

Shaw, R.H., U. Schumann and J. Graf, 1991: Large eddy simulation of turbulent flow above and within a forest. Proc. 20th Conference on Agricultural and Forest Meterology, Sept. 10-13, 1991, Salt Lake City, Utah, paper 2.4, 4 p.

Smolarkiewicz, P.K., 1984: A fully multidimensional positive definite advection transport algorithm with small implicit diffusion. *J. Comput. Phys.* **54**, 325-362.

Smolarkiewicz, P.K. and T.L. Clark, 1986: The multidimensional positive definite advection transport alpgorithm: Further development and applications. *J. Comput. Phys.* **67**, 396-438.

Smolarkiewicz, P.K. and W.W. Grabowski, 1990: The multidimensional positiv definite advection transport algorithm: nonoscillatory option. *J. Comput. Phys.* **86**, 355-375.

Sommeria, G., 1976: Three-dimensional simulation of turbulent processes in an undisturbed trade wind boundary layer. *J. Atmos. Sci.* **33**, 216-241.

Sorbjan, Z., 1990: Similarity scales and universal profiles of statistical moments in the convective boundary layer. *J. Appl. Met.* **29**, 762-775.

Sorbjan, Z., 1991: Evaluation of local similarity functions in the convective boundary layer. *J. Appl. Met.* **30**, in press.

Speziale, C.G., 1985: Galilean invariance of subgrid-scale stress models in large eddy simulation of turbulence. *J. Fluid Mech.* **156**, 55-62.

Stull, R.B., 1988: *An Introduction to Boundary Layer Meteorology*. Kluwer, Dordrecht, 664 pp.

Sykes, R.I. and D.S. Henn, 1989: Large-eddy simulation of turbulent sheared convection. *J. Atmos. Sci.* **46**, 1106-1118.

Walko, R.L., W.R. Cotton and R.A. Pielke, 1990: Large eddy simulation of the CBL over hilly terrain. *Proc. 9th Symposium on turbulence and diffusion*. Roskilde, Denmark, April 30 - May 3, Amer. Meteorol. Soc., Boston, Mass., p. 409-412.

Wyngaard, J.C., 1987: A physical mechanism for the asymmetry in top-down and bottom-up diffusion. *J. Atmos. Sci.* **44**, 1083-1087.

Wyngaard, J.C. and R.A. Brost, 1984: Top-down and bottom-up diffusion of a scalar in the convective boundary layer. *J. Atmos. Sci.* **41**, 102-112.

Wyngaard, J.C. and J.C. Weil, 1991: Transport asymmetry in skewed turbulence. *Phys. Fluids*, A **3**, 155-162.

Young, G.S., 1988: Turbulence structure of the convective boundary layer. Part II: Phoenix 78 aircraft observations of thermals and their environment. *J. Atmos. Sci.* **45**, 727-735.

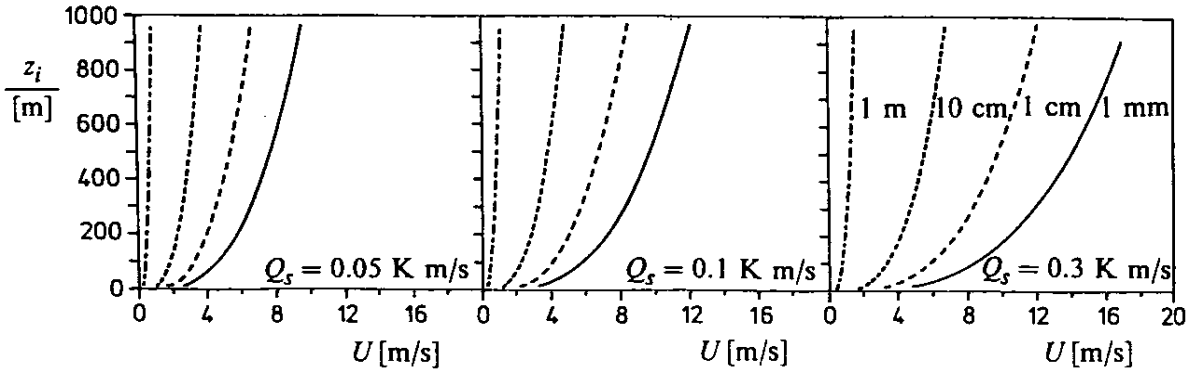

Fig. 1 maximum windspeed U at height $2m$ versus boundary layer depth z_i for which the boundary layer can be treated as a convective boundary layer (CBL), i.e. for which $z_i/(-L) \geq 5$. Parameters are (from left to right) $Q_s = 0.05$, 0.1, 0.3 K ms^{-1}, and the roughness height $z_0 = 1$ m, 10 cm, 1 cm, 1 mm.

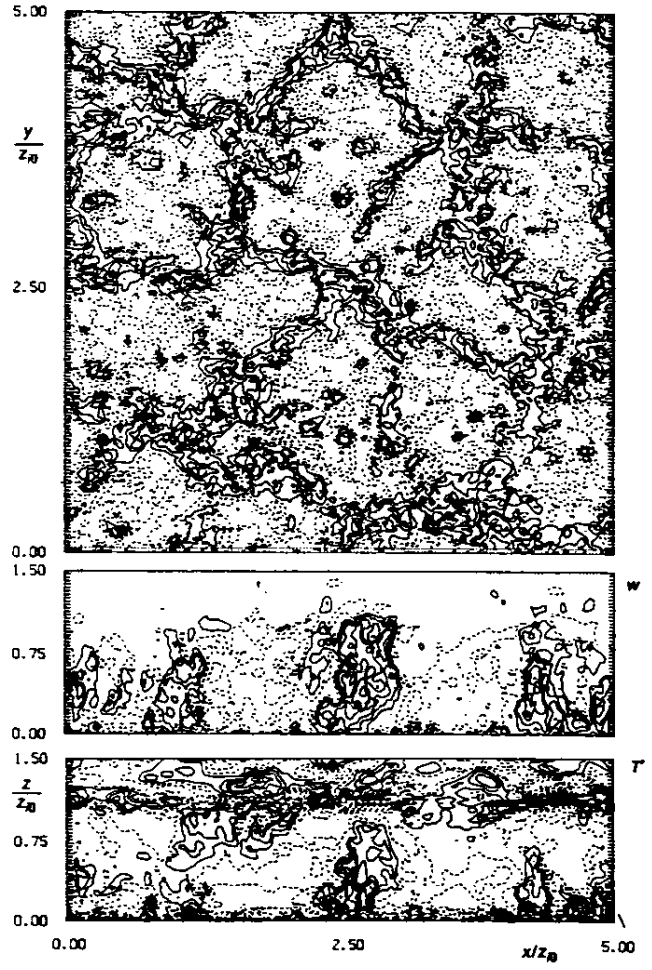

Fig. 2 Vertical velocity fluctuation w' in a horizontal cross-section at $z/z_i = 0.25$ (top), and, together with temperature fluctuations T', in a vertical cross-section (bottom), from Schmidt and Schumann (1989).

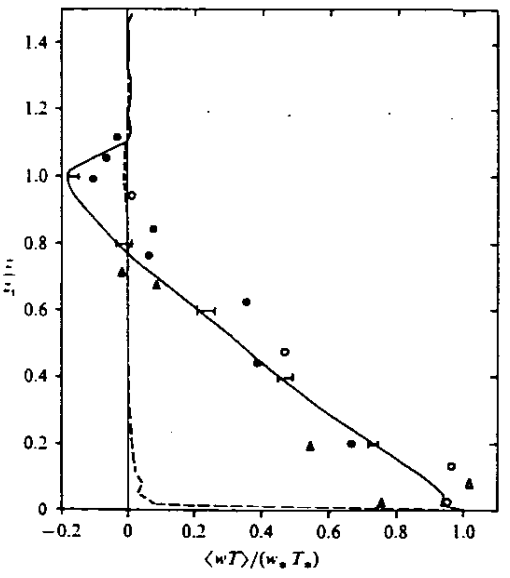

Fig. 3 Vertical temperature flux $\langle w'T' \rangle$ versus height z (Schmidt and Schumann 1989). Full curve: LES result, error bars denote standard deviation; dashed curve: mean SGS flux; full symbols: laboratory measurements; open symbols: aircraft measurements.

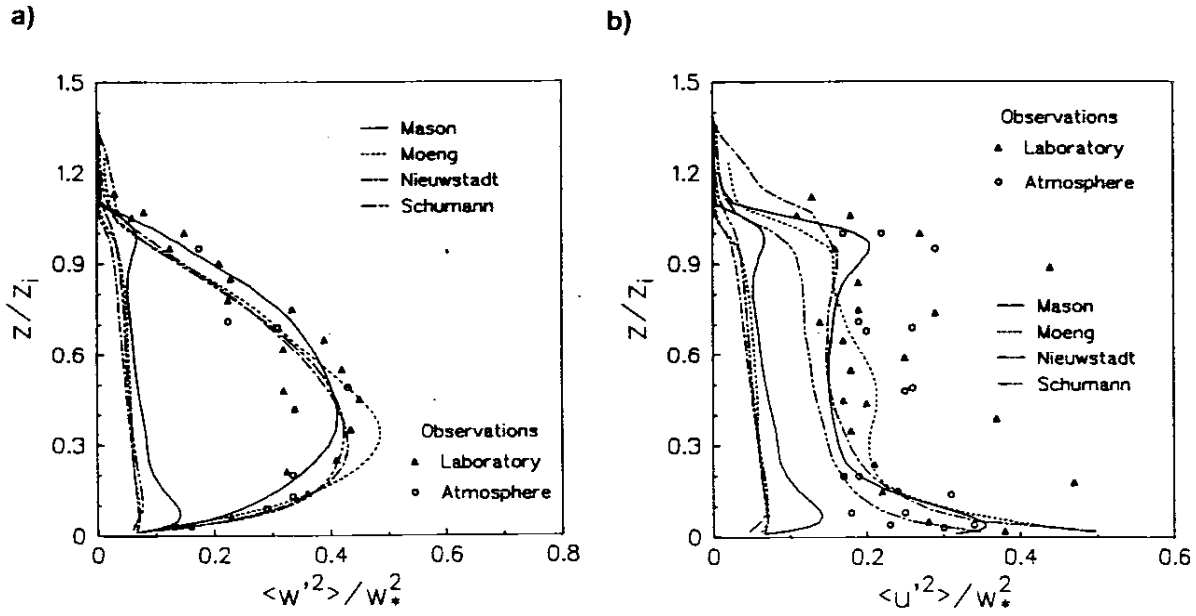

Fig. 4 Variances of velocity fluctuations versus height z_i, from Nieuwstadt et al. (1991). Total variances and SGS parts. a) Left: vertical velocity variance, b) right: horizontal velocity variance.

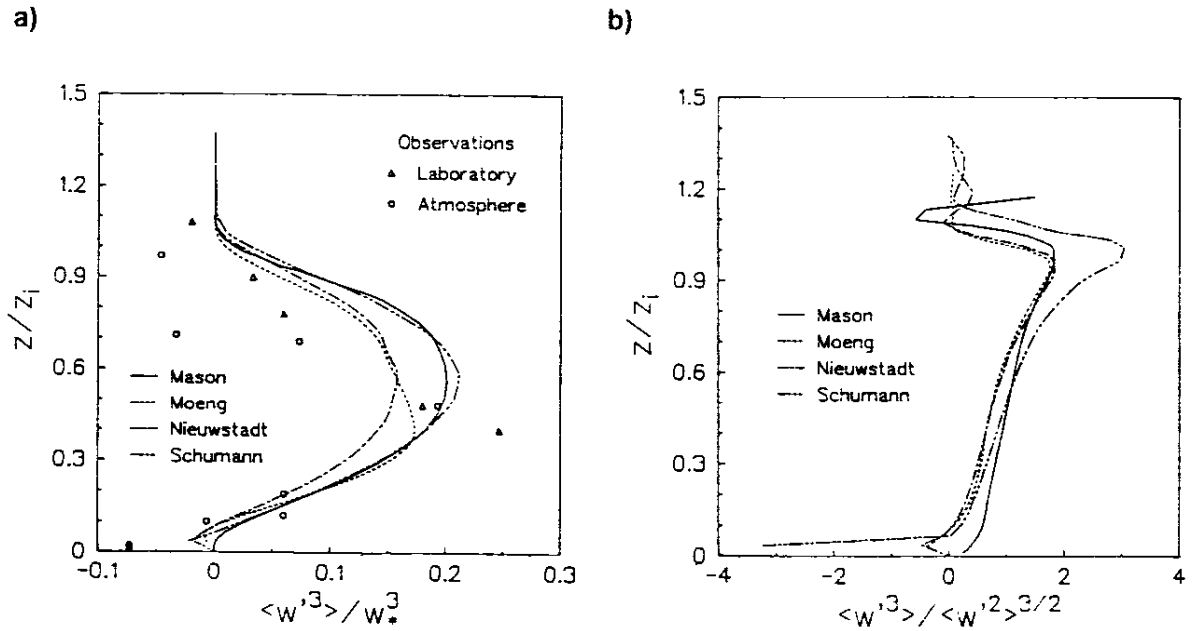

Fig. 5 a) Third moment of the vertical velocity fluctuations versus height. b) Skewness S versus height (Nieuwstadt et al. 1991).

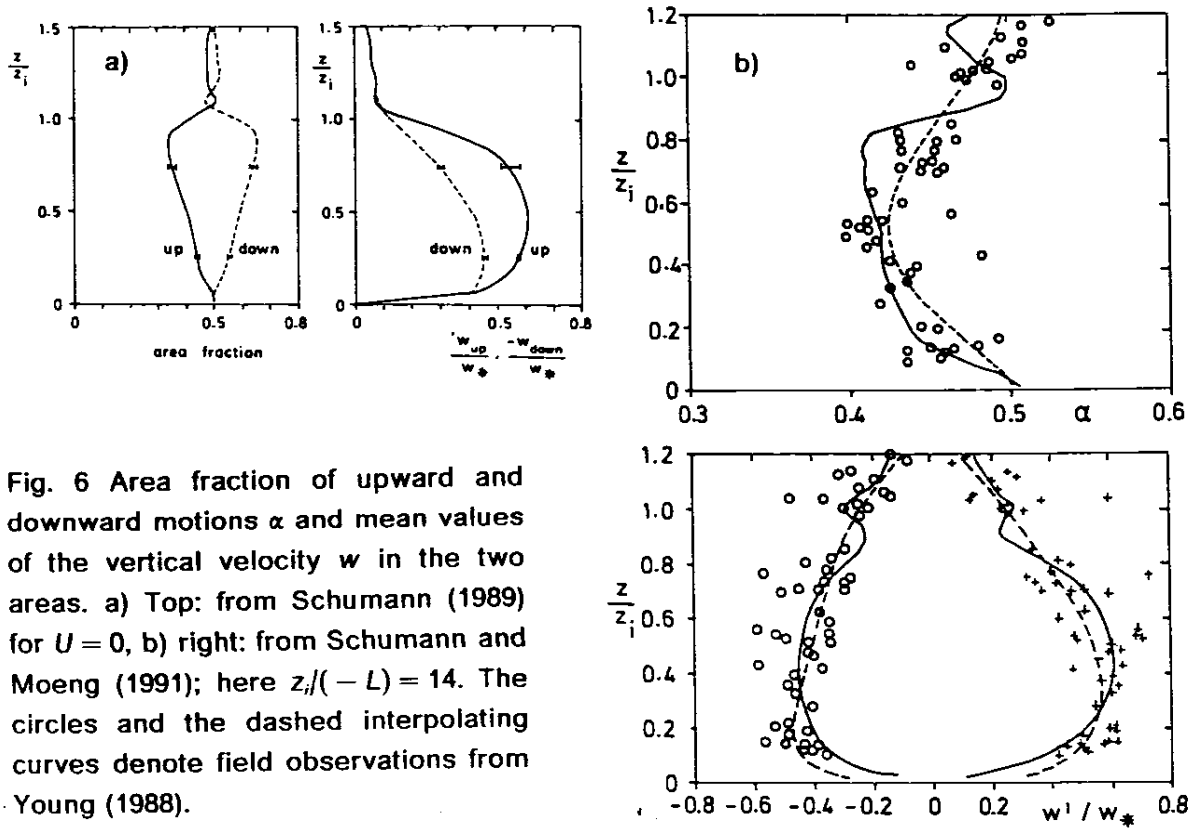

Fig. 6 Area fraction of upward and downward motions α and mean values of the vertical velocity w in the two areas. a) Top: from Schumann (1989) for $U = 0$, b) right: from Schumann and Moeng (1991); here $z_i/(-L) = 14$. The circles and the dashed interpolating curves denote field observations from Young (1988).

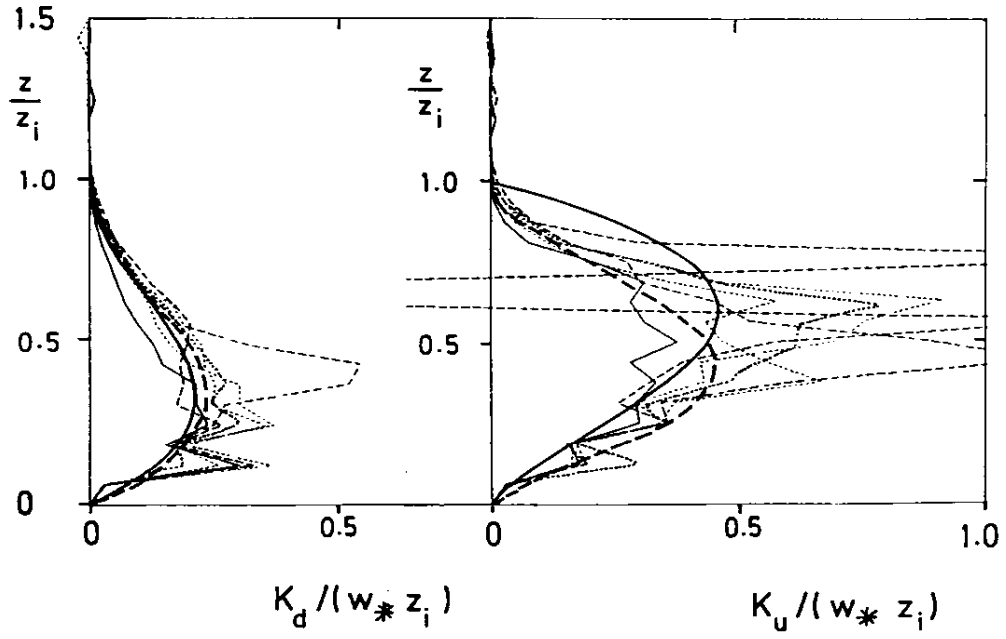

Fig. 7 Effective eddy-diffusivites for top-down (K_d) and bottom-up (K_u) diffusivity versus height at a sequence of times. Dotted curves: mean value; thick curves: interpolations from Moeng and Wyngaard (1984); dashed curves: interpolation from Schumann (1989).

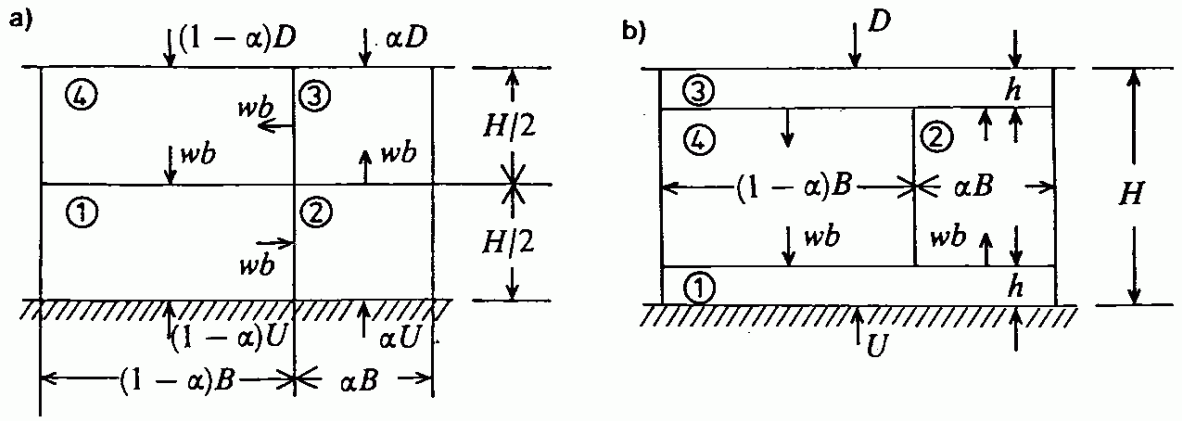

Fig. 8 Sketch of simple flow configurations for estimates of vertical diffusion. Here, $\alpha \equiv \alpha_u$ denotes the updraft area fraction.

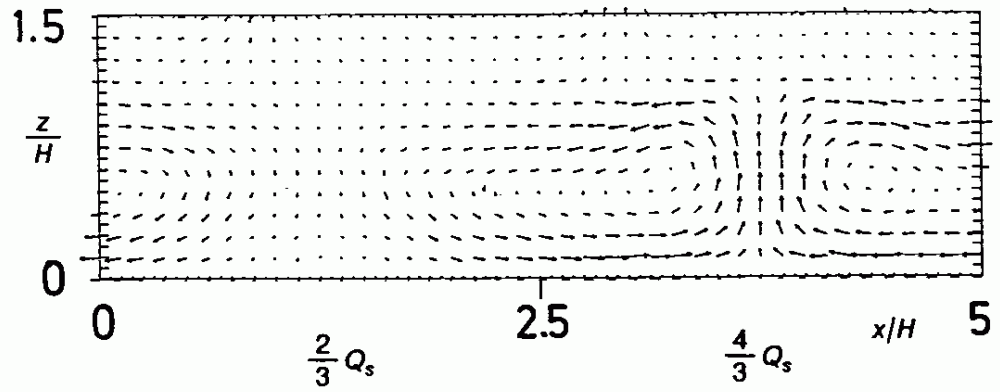

Fig. 9 Mean velocity vector field in a vertical cross-section of a CBL over a flat surface with step-wise varying surface heat flux.

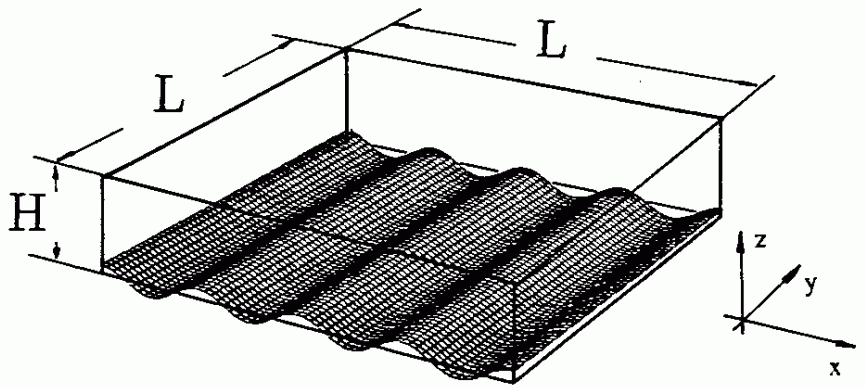

Fig. 10 Perspective plot of the computational domain as used for LES of convection over wavy terrain. In the example the surface wave has amplitude $\delta = 0.1H$, and wavelength $\lambda = H$; $L = 4\lambda$.

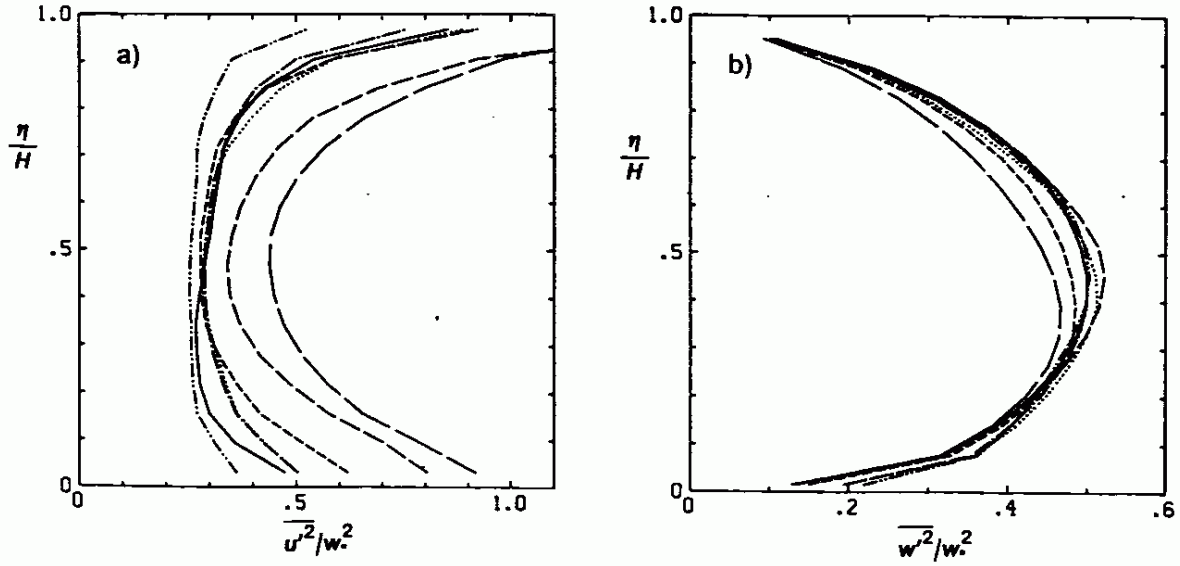

Fig. 11 LES results for mean profiles of a) variance of velocity in x-direction, b) same in z-direction. ..... L1014, —— L1024, __ __ L1044, _____ L00U4, _.._.. L1514, –.–. L1018, ___ ___ L1088.

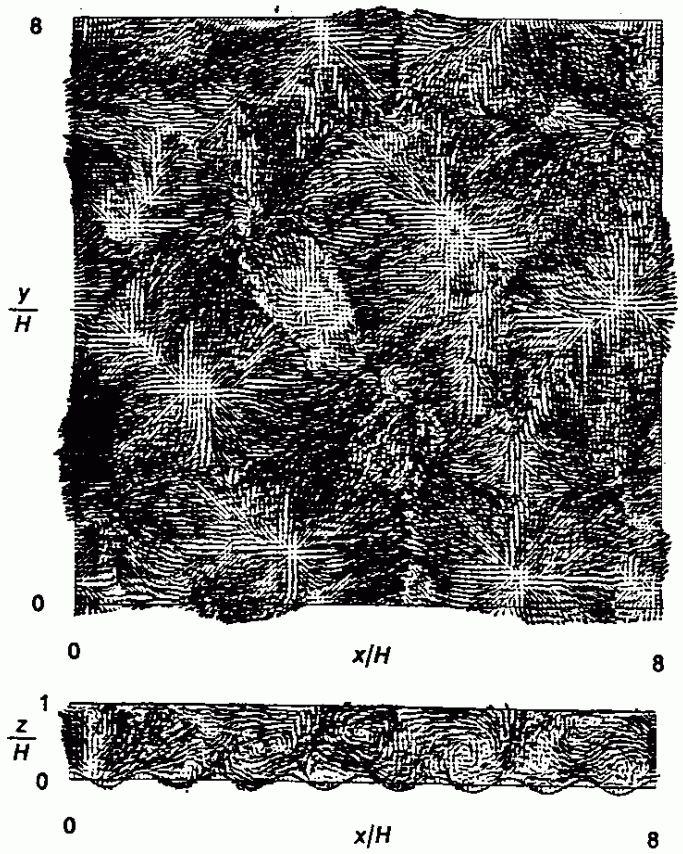

Fig. 12 Velocity field at $z = H$ (top) and at $y = 0$ (bottom), averaged from $t/t_* = 30$ to 35 in the case with $L/H = 8$, $\lambda = H$, $\delta = 0.1$ (case L1018). Maximum velocity 1.72 w_*.

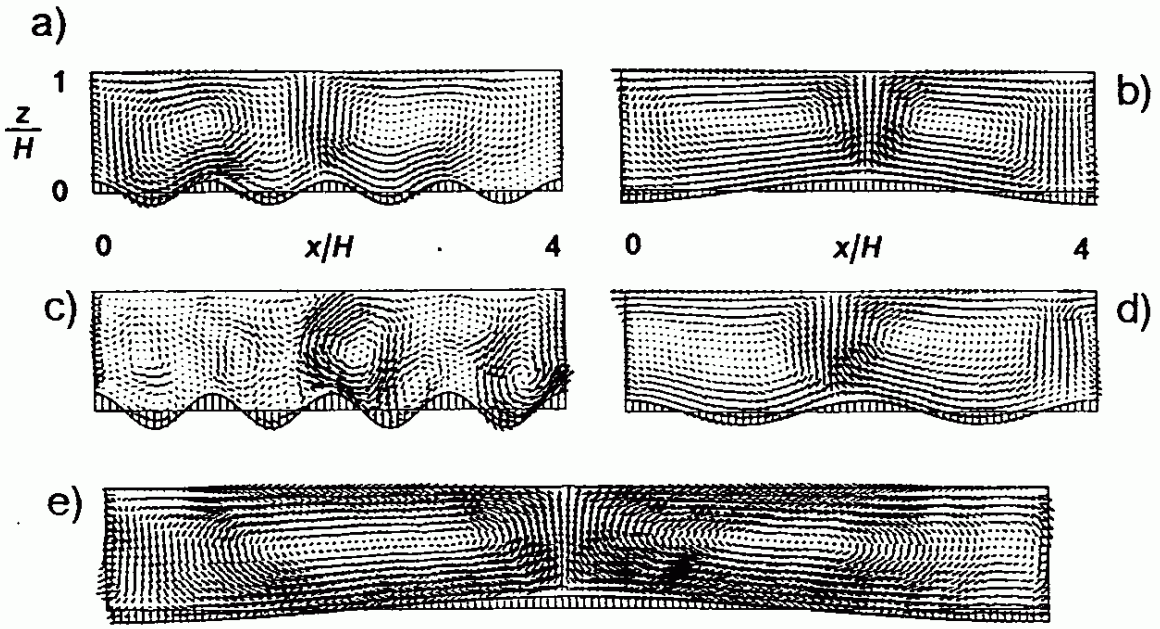

Fig. 13 Influence of wavelength of orography on the velocity field in a vertical plane for various surface undulations. These plots represent time and y-averaged results. a) L1014, b) L1044, c) L1514, d) L1024, e) L1088. Maximum normalized velocity vectors a) 1.03, b) 1.34, c) 1.32, d) 0.62, e) 1.0.

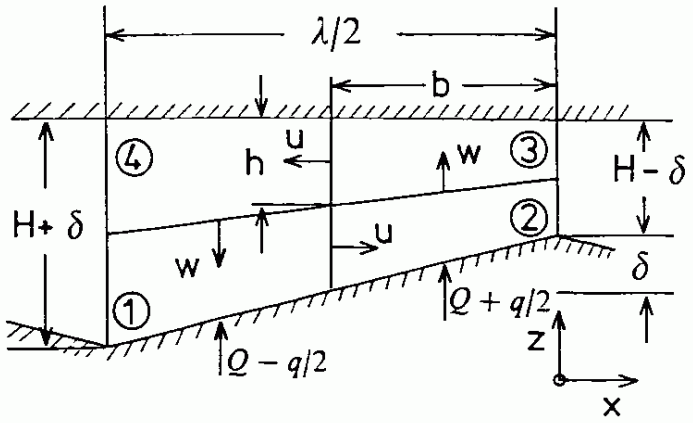

Fig. 14 Sketch of a half-wave (wavelength $\lambda = 4b$) of a vertical cross-section of the periodic flow domain of mean height $H = 2h$ with surface height amplitude δ and mean variations in surface temperature flux $Q \pm q/2$, showing the four control volumina 1 to 4, and characteristic horizontal and vertical velocities u and w.

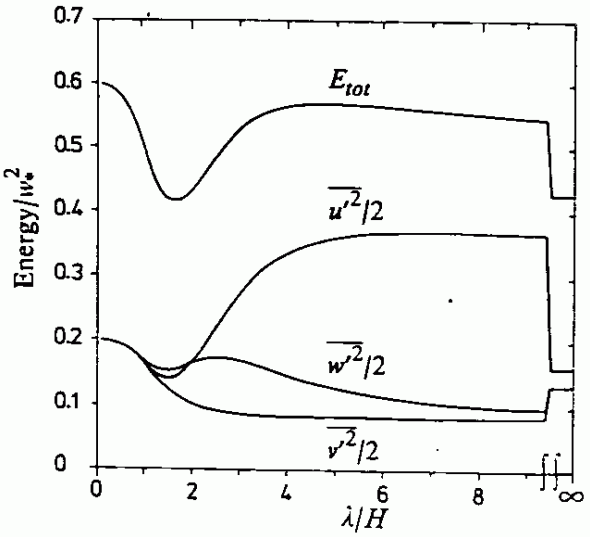

Fig. 15 Total energy E_{tot}, and energies of the three velocity components. Lateral: $v'^2/2$, vertical: $v'^2/2 + \gamma w^2/2$, and horizontal: $v'^2/2 + \gamma u^2/2$, versus wavelength λ/H, for $q/Q = 0$, $\delta/H = 0.1$, $z_0/H = 10^{-4}$, $\alpha = 0.079$.

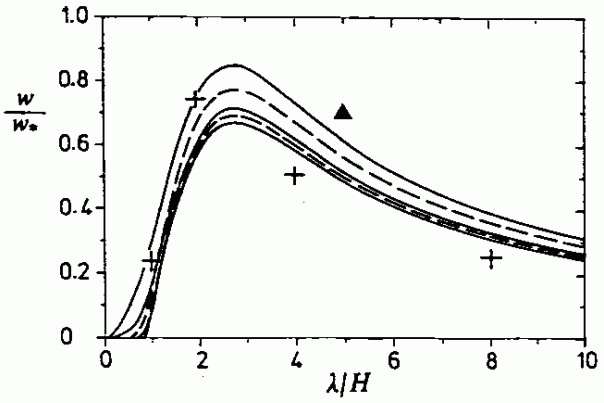

Figure 16. Vertical convection velocity w/w_* versus wavelength λ/H for various values of terrain amplitude $\delta/H = 0$, 0.1, and 0.5, with homogeneous surface heating, $q/Q = 0$ (full curves), and for various values of surface heating $q/Q = 0$, 0.1, and 0.5, with $\delta/H = 0$ (dashed curves); $\alpha = 0.079$. The crosses denote the present LES results (average of maximum mean updraft and maximum mean downdraft velocity) for $\delta/H = 0.1$. The triangle denotes the result from a case with flat surface but variable surface heating ($q/Q = 2/3$).

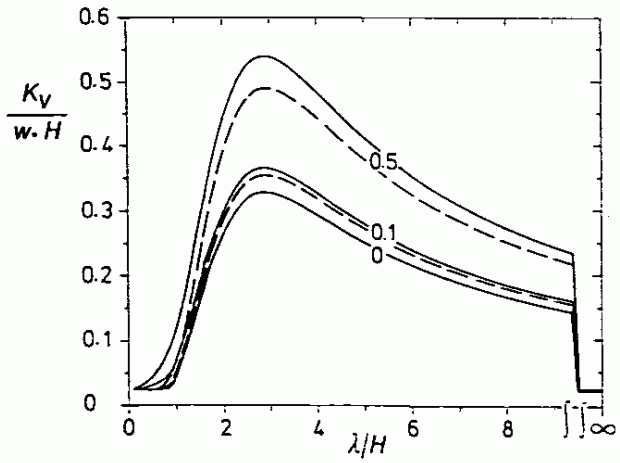

Fig. 17 Vertical effective diffusivity $K_v/(w_*H)$ versus wavelength λ/H for various values of terrain amplitude $\delta/H = 0$, 0.1, and 0.5, with $q/Q = 0$ (full curves), and for various values of surface heating $q/Q = 0$, 0.1, and 0.5, with $\delta/H = 0$ (dashed curves). Asymptotic solutions for $\lambda/H = 1000 \cong \infty$ are indicated at the right vertical axis; $z_0/H = 10^{-4}$, $\alpha = 0.079$.